

Review

Recent progress of organic photovoltaics for indoor energy harvesting

Lin Xie ^{a,b}, Wei Song ^a, Jinfeng Ge ^a, Bencan Tang ^{b,*}, Xiaoli Zhang ^c, Tao Wu ^b, Ziyi Ge ^{a,*}^a Ningbo Institute of Materials Technology and Engineering, Chinese Academy of Sciences, Ningbo 315201, PR China^b Department of Chemical and Environmental Engineering, Faculty of Science and Engineering, University of Nottingham Ningbo China, Ningbo 315100, PR China^c School of Materials Science and Engineering, Zhengzhou University, 450001 PR China

ARTICLE INFO

Keywords:

Indoor energy harvester
Indoor organic photovoltaics
IoT
Indoor environment
LED
Weak illuminance

ABSTRACT

The recent progress of indoor organic photovoltaics (IOPVs) is reviewed in this work for abundant low power consumption applications. In recent years, organic solar cells have attracted significant attention to harvest solar energy. However, many drawbacks of such as discontinuous adequate sunlight, heat instability, and strong illumination instability inhibit outdoor organic photovoltaic technology from entering solar panel market. As the market of IoT nodes (e.g. sensors, watches, calculators, remote control, hearing aid, and monitors) used in relatively mild indoor environment rapidly grows, the demand for artificial light energy harvesters to supply continuous and cordless power for the indoor environment has emerged. Organic photovoltaic technology for indoor harvesters is one of the reliable candidates because the energy level of organic materials is tunable to match the indoor light source spectra so that its power conversion efficiency (PCE) outweighs that of most of the other indoor harvesters. Indoor organic photovoltaics exhibit the PCE over 30% with an output power of 150 μWcm^{-2} under the illuminance of artificial lights, which is high enough to drive numerous indoor applications. This review summarizes the performance mechanism of organic photovoltaics (OPVs) when the illuminance is switched from 1-sun to dim light, the research progress for indoor energy transformation, and the viewpoint to speed up the development of IOPVs.

1. Introduction

Clean energy plays a significant role to replace gradually exhausted non-renewable energy resources, such as fossil fuel, thus, unprecedented demand for energy harvesting technologies utilizing sustainable energy has been reported [1–4]. Various solar power harvesters that convert solar energy to power have attracted dramatic attention nowadays. Among abundant types of photovoltaics (PVs), organic solar cells (OSCs) have unique advantages including tunability of energy level, flexibility, low-cost, transparency, lightweight, and large-area roll to roll processability [5–7]. These advantages make the prospects of OSCs surpass traditional silicon-based solar cells in the near future [8]. In terms of OSCs' PCEs, the maximum certificated power conversion efficiency (PCE) has reached 17.6% under 1-sun illuminance by now [9].

In the laboratory, a standard testing condition (AM1.5) that simulates the spectrum of the sun with an intensity of 100 mW cm^{-2} is universally adopted to evaluate the photoelectric properties of solar cells [10]. However, adequate sunlight is not always available, especially during rainy days, nights, and winter. Furthermore, photovoltaic

technologies can be used not only for outdoor applications, such as traditional solar plants, household rooftop solar systems, public lighting, solar-powered transportation, but also for indoor devices to utilize indoor light sources comprising wearable solar technology, portable electronics, and the Internet of Things (IoTs) as described in Fig. 1(a) [11–13]. The definition of IoTs is automatically wireless communication between unique identifiers of things (various electronic devices) via the internet. Realtime data and digital information can be collected and exchanged through terminal devices, sensors, health monitors, and so on, which are adopted for smart homes, factories, retail sectors, and wearable technology. This huge amount of applications which are independent and off-the-grid require abundant power supplier to operate. To replace non-self-rechargeable batteries that drive indoor applications at intervals is non-automatic and unintelligent. Therefore the successive power supplement via indoor photovoltaics (IPVs) which harvest energy from ambient lighting source is necessary in the near future [14]. Numerous studies about IPVs have been carried out. The artificial indoor lighting sources include light-emitting diodes (LEDs), compact fluorescent lamps (CFL), halogen lamps, and incandescent light bulbs. The

* Corresponding authors.

E-mail addresses: Bencan.Tang@nottingham.edu.cn (B. Tang), geziyi@nimte.ac.cn (Z. Ge).

spectra of differently and frequently used dim lights are illustrated in Fig. 2. The optical spectra for indoor light sources are mainly distributed from 400 nm to 750 nm, which are similar to the visible spectrum region of human eyes. The detail spectrum is dependent on the specific light source, color rendering and intensity.

The promising and rising market for IPVs by utilizing the micro energy derives from the huge demand for energy-autonomous applications. In 2017, the business markets for IPVs was only \$ 140 million, which was far below \$ 100 billion market for solar power devices. However, the quickly rising demand for IPVs for indoor applications boosts the market growth, and the global market for annual IPVs is predicted to be over \$ 850 million by 2023 and has the potential to keep growing in the following years [14].

Although there are a few studies of IPVs, comprising indoor organic photovoltaics (IOPVs) [16–22], crystallized Si cells [23,24], dye-sensitized solar cells [16,17,25,26], perovskite solar cells [27–34], and III–V compound semiconductor cells- GaAs [15,23], we only provide the recent progress of IOPVs. As IOPVs possess outstanding properties of readily tunable chemistry and physics and have good prospect of eco-compatible processability of large area and flexibility. Crystalline silicon cells achieve good result for harvesting solar energy, but their PCEs under dim ambient are not desirable which is discussed in Section 2.1. In the aspect of perovskite cells, they show outstanding PCEs under conditions of AM1.5 and dim light. Due to sharing abundant material advantages of organic photovoltaics (OPVs), perovskite photovoltaics are often regarded as a potential competitor of OPVs. In comparison with PCEs of IOPVs which mostly distributed below 25%, large portion of PCEs for perovskite cells under indoor conditions are over 25%, and some are over 30% [30,32,33]. However, the toxic lead content is a persistent threat in sustainable development and a hinder for commercialization [35]. Dye-sensitized photovoltaics show comparable performance with IOPVs under weak illumination, but it is difficult to eliminate the use of notably platinum and ruthenium as electrodes, which is not prefer for commercialization. Moreover, liquid electrolyte has drawbacks of temperature instability and constituent of volatile organic compounds which suffers the difficulties of large area producibility and flexibility [36]. Fig. 1(b) illustrates the low power requirements for various indoor wirelessly interconnected devices supplied by a 1 cm² IPV cell, which prove that IPVs are promising candidates to harvest energy under weak light conditions. For example, the PCE of IOPVs so far is around 30% with the input power of 0.5021 mW cm⁻², hence, the output power is equal to ca. 15 μW cm⁻² which is adequate to drive many electronic applications [37].

In this review, following this introduction section, we summarize the

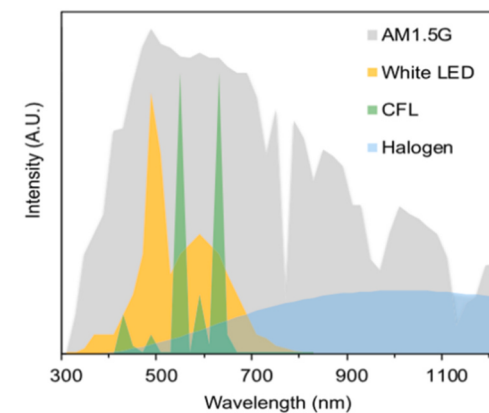


Fig. 2. Output spectra of different light sources: AM1.5 (gray), white LED (orange), CFL (green), halogen [14] with permission from Elsevier (Copyright 2019). (For interpretation of the references to colour in this figure legend, the reader is referred to the web version of this article.)

principles of achieving high efficiency in indoor environment. Subsequently, the method of IOPVs performance characterization is outlined, where the reason why spectrometer is used to ensure the incident light intensities rather than lux meter is explained. Next, the reviews of progress are carried out to show the big progress achieved for IOPVs technology. Finally, the perspectives are provided to accelerate the IOPVs' development.

2. Principles to achieve high efficiency of IOPVs

2.1. Theoretical maximum PCE for IPVs

According to the detailed balance limit theory, the maximum PCEs based on theoretical calculations for photovoltaics by the methodology of Shockley and Queisser [41] are shown in Fig. 3(a) [38]. The corresponding calculation for theoretical maximum PCEs based on different light sources is on the assumption that energy above the material bandgap is all absorbed, and the carriers are fully extracted. Theoretical calculations reveal that the optimal bandgap for indoor light sources is ca. 1.9 eV, whereas the optimal bandgap energy for AM1.5 is ca. 1.34 eV [16,41]. The wider bandgap material is, the better spectra of indoor light are covered. According to Fig. 3(a), for phosphor and 3-color LEDs, the maximum theoretical efficiency is close to 60% at the bandgap of 1.9 eV,

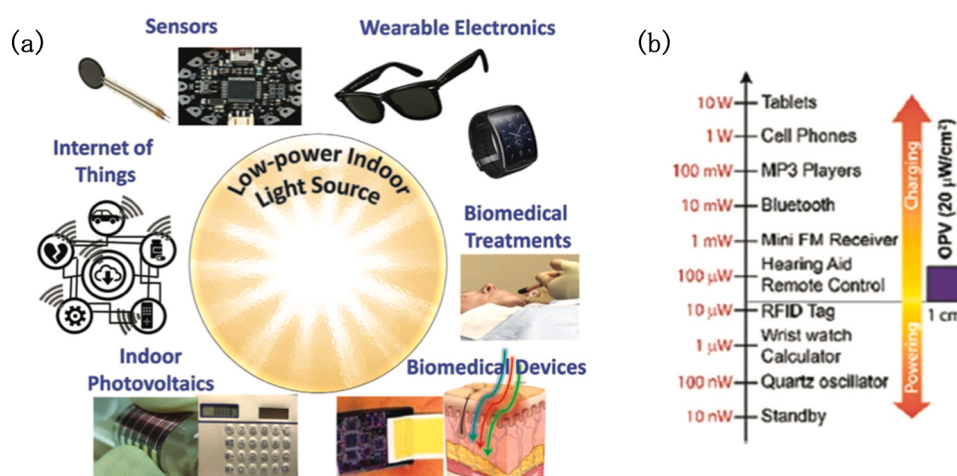


Fig. 1. (a) Devices acquire power from indoor photovoltaics under dim lighting conditions [15] with permission from John Wiley and Sons (Copyright 2018). (b) Electrical energy requirements for various application devices supplied by a 1 cm² IPV cell under indoor lighting conditions [15] with permission from John Wiley and Sons (Copyright 2018).

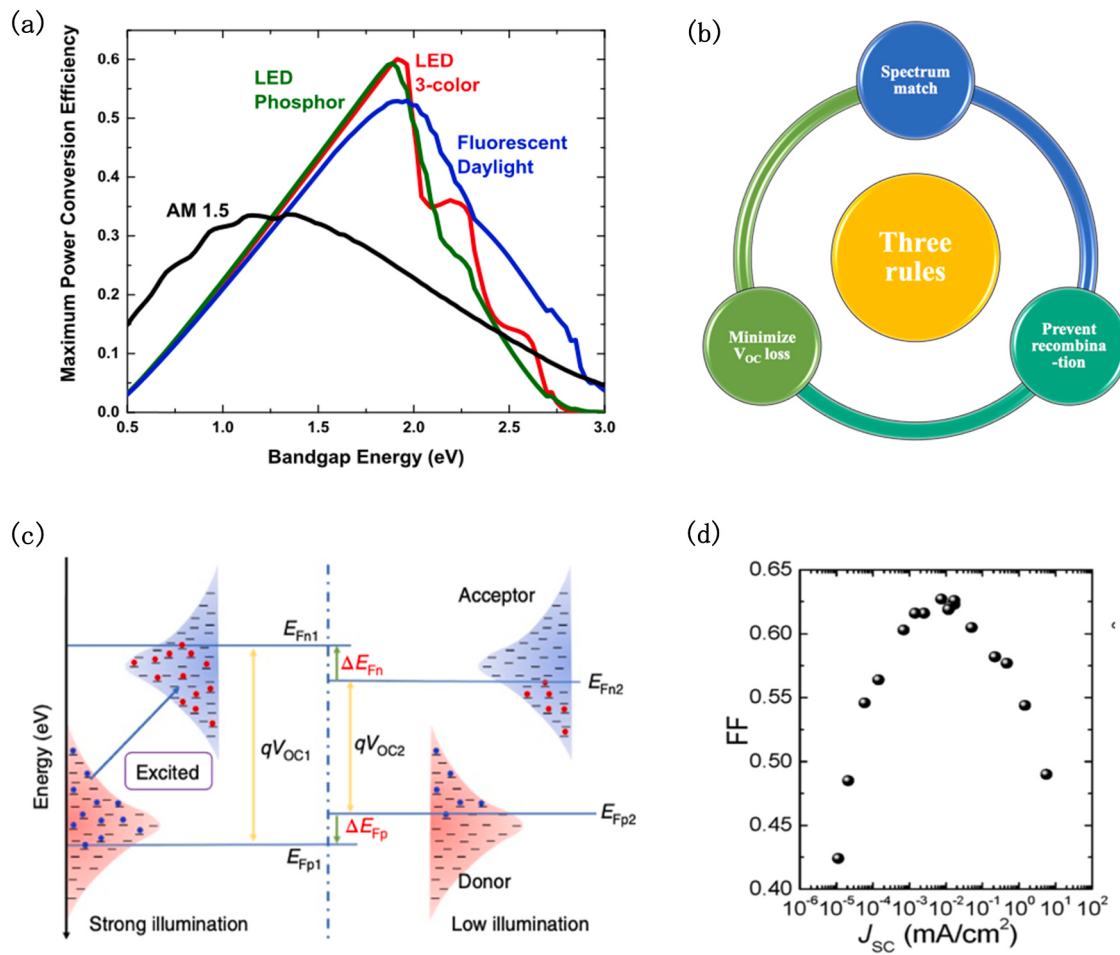


Fig. 3. (a) Bandgap of active material dependent theoretical maximum PCE under different lighting sources demonstrating an ideal bandgap energy near 1.9 eV for ambient conditions [38]. Copyright 2015, IEEE. (b) Three rules in order to achieve high PCE for IPV under indoor lighting sources. (c) The quasi-Fermi levels of donors and acceptors under strong and weak illuminations [39]. Copyright 2019, Nature energy. (d) The variation of FF is dependent on the J_{SC} [40] with permission from Royal Society of Chemistry (Copyright 2014).

however, the upper-limit calculative efficiency for AM1.5 doesn't exceed 40% at the bandgap of 1.34 eV. This is because the spectra of the indoor light sources are narrow so that the photons of irradiance can be sufficiently utilized by active materials. Moreover, the narrower band of spectra, the less transparency and thermalization losses [38]. The bandgap of crystalline silicon is ca. 1.1 eV which corresponds to the optimal bandgap under solar illuminance, hence, silicon-based cells can achieve impressive efficiency under the AM1.5. On the contrary, silicon-based cells with narrower bandgap produce lower PCE for the indoor lighting conditions compared with OPVs [18,22,42,43]. Although PCE of OPVs is lower than that of the crystalline silicon cells under solar simulator owing to low absorption in the near infrared (NIR) region, sufficiently transferring photons and tunable bandgap make IOPVs acquire higher efficiency under indoor illumination conditions with narrower spectra and weaker intensities. Due to the tunable bandgap of organic material based on molecular design, the photoelectric properties of IOPV can get closer and closer to the maximum theoretical efficiency under dim light. In sum, the bandgap of organic active material should be designed and synthesized being close to ca. 1.9 eV to maximize the PCE in indoor environment.

2.2. Three important rules

To achieve a high PCE, three rules, displayed in Fig. 3(b), are suggested to be applied. The first rule is that the photoresponse of the active material should maximally match the spectrum of the indoor light

source. For OSCs under AM1.5, the low-bandgap active material is pursued to extend the absorption edge in the NIR region [44] and the maximal PCE is approaching 18% [9]. When testing these high efficiency of OSCs in indoor condition, their efficiency cannot be improved significantly because of the emission power spectra of LED and CFL range approximately from 400 to 750 nm, whose intensities are smaller than 1 mW cm^{-2} [45]. Therefore, the optimally overlapped spectra between emission and absorption are critical, which can sufficiently transfer the incident photons into the light current, thereby minimizing transparency losses. In addition, a high external quantum efficiency (EQE) is also necessary to mitigate the thermalization of photogenerated charges [39].

The second rule is that the loss of V_{OC} should be suppressed as much as possible. When the 1-sun illumination is changed to indoor lighting conditions, the V_{OC} of devices decreases unavoidably, because the intensities of lighting sources drop significantly. V_{OC} is defined by the electron and hole quasi-Fermi levels of semiconductors [46]:

$$V_{OC} = 1/q(E_{Fn} - E_{Fp}) \quad (1)$$

Where q is the elementary charge, E_{Fn} is the electron quasi-Fermi levels and E_{Fp} indicates hole quasi-Fermi levels. As displayed in Fig. 3(c), E_{Fn} and E_{Fp} are correlative to the illumination intensities of lighting sources. Decreasing light intensity, E_{Fn} shifts up and E_{Fp} shifts down, which explains why the illuminances declination leads to the decrease of V_{OC} [47]. How to make sure the V_{OC} is large in dim light conditions is

essential for achieving high PCE. The relationship between the V_{OC} and photocurrent is shown [46,48–50]:

$$V_{OC} = \frac{nKT}{q} \ln \left[\frac{I_{ph}(V_{OC})}{I_0} + 1 - \frac{V_{OC}}{R_{sh} I_0} \right] \approx \frac{nKT}{q} \ln \left[\frac{I_{ph}}{I_0} \right] \quad (2)$$

Where n is the ideality factor (assumption as 1), k is the Boltzmann constant, T is the cell temperature, q is the electron charge, R_{sh} is the shunt resistance, and I_0 is the reverse dark saturation current. Based on this expression, So' group concluded that minimizing the I_0 can contribute to maximize V_{OC} [19].

Under 1 sun condition, the leakage current is 3 order magnitudes less than , so the R_{sh} of $10^4 \Omega \text{ cm}^2$ is enough to maintain V_{OC} . Under dim lighting conditions, the carrier density is extremely low and the leakage current plays an important role that impact the V_{OC} [37,51]. Stein's group [52] suggested that a minimum R_{sh} of $85,000 \Omega \text{ cm}^2$ and maximum series resistance (R_s) of $50 \Omega \text{ cm}^2$ are necessary for IOPVs under weak light conditions. On the contrary, a R_{sh} of $1000 \Omega \text{ cm}^2$ or higher and a R_s of $3 \Omega \text{ cm}^2$ or lower are required to acquire high efficiency for outdoor solar cells. Integrated OPV cells, which are applied in both, indoor and outdoor environment, need a R_{sh} of $85,000 \Omega \text{ cm}^2$ or higher and a R_s of $3 \Omega \text{ cm}^2$ or lower. Furthermore, the loss of V_{OC} under room light is shown as:

$$\Delta V = \frac{nKT}{q} \ln \frac{I_{ph,sun}}{I_{ph,room}} \quad (3)$$

Where $I_{ph,sun}$ and $I_{ph,room}$ represent the photocurrents under AM1.5 and indoor illuminance conditions, respectively. Normally, I_{ph} increases with the increment of incident illuminance power (P). P_{sun} (100 mW cm^{-2}) is the illuminance intensity of the sun, and P_{room} is the illuminance intensity under indoor environment. Hence $P_{sun}\theta$ means the illuminance power of solar spectrum without infrared region. θ is the fraction of light corresponding the wavelength smaller than 780 nm (the upper limit of the photopic region). Therefore, the Eq. (3) can be rewritten as:

$$\Delta V \approx \frac{nKT}{q} \ln \frac{P_{sun}\theta}{P_{room}} \quad (4)$$

Hence, simulate V_{OC} under indoor lighting sources can be expressed as:

$$V_{OC,room} \approx V_{OC,sun} - \frac{nKT}{q} \ln \frac{P_{sun}\theta}{P_{room}} \quad (5)$$

So' group compared V_{OC} s of one specific OPV device under the solar spectrum without infrared region and under the 300-lux indoor light source, respectively, resulting in a computed $\Delta V \approx 0.166 \text{ V}$. In other words, when the OPV is brought from solar illuminance to dim illumination, an additional V_{OC} loss of ca. 0.166 V is unavoidable. For OPVs under 1-sun illumination, the energy loss (E_{loss}) arises from free carrier recommendation losses and the charge transfer (CT) losses. The reported E_{loss} in the most efficient OSCs is typically $0.5\text{--}0.6 \text{ eV}$ under AM1.5 [53, 54]. E_{loss} is the offset between the optical bandgap of acceptor and the measured qV_{oc} which is written as:

$$E_{loss} = E_g - qV_{oc} \quad (6)$$

Where E_g is the optical bandgap derived from the absorption onset λ_{onset} ($= 1240/\lambda_{onset}$). Hence, we can assume that the total V_{OC} loss is $0.666\text{--}0.766 \text{ V}$ under indoor conditions as the extra V_{OC} loss of 0.166 V is unavoidable when lighting conditions are changed from 1 sun to dim lights. Therefore, we can conclude that a high V_{OC} under AM1.5 and a small V_{OC} loss in indoor environment are essential for IOPVs to achieve a high V_{OC} under indoor environment. If a wide bandgap material has E_g of 1.8 eV , a high V_{OC} of ca. 1 V under artificial lights are achievable.

Thirdly, when the intensities decrease from AM1.5 to indoor light conditions, the carrier density dramatically declines, at which trap-

assisted recombination significantly suppresses electrodes to efficiently collect charge carriers. [45,55–57]. Under weak light intensity, trap can impact not only short circuit current (J_{SC}) and V_{OC} , but also filling factor (FF) [40,58]. Therefore, prevent trap-assisted recombination is vital in achieving high PCEs for IOPVs. As displayed in Fig. 3(d), Kippelen et al. pointed out that FF initially increased with increase of J_{SC} that effected by illuminance [40]. However, with the further increase of J_{SC} , FF gradually declined. Kippelen et al. explained that FF is as a function of $\nu_{OC} = \frac{qV_{OC}}{nKT}$, $r_s = \frac{R_s}{R_{ch}}$ (where $R_{ch} = \frac{V_{OC}}{J_{SC}A}$), and $r_{sh} = \frac{R_{sh}}{R_{ch}}$, which is detailed expressed in the following semi-empirical equations:

$$\begin{aligned} FF_0 &= \frac{\nu_{OC} - \ln(\nu_{OC} + 0.72)}{\nu_{OC} + 1} \quad \left(R_s = \frac{1}{R_{sh}} = 0 \right), \\ FF_S &= FF_0(1 - 1.1r_s) + 0.19r_s^2 \quad \left(0 \leq r_s \leq 0.4, \quad \frac{1}{r_{sh}} = 0 \right), \\ FF &= FF_{SP} = FF_S \left\{ 1 - \frac{(\nu_{OC} + 0.7)}{\nu_{OC}} \frac{FF_S}{r_{sh}} \right\} \quad \left(0 \leq r_s + \frac{1}{r_{sh}} \leq 0.4 \right) \end{aligned} \quad (7)$$

In the weak illumination, where J_{SC} is less than $10^{-2} \text{ mA cm}^{-2}$, results in $r_s \approx 0$, thus $FF_S \approx FF_0$, and $FF \approx FF_0(\nu_{OC}) \left\{ 1 - \frac{(\nu_{OC} + 0.7)}{\nu_{OC}} \frac{FF_0(\nu_{OC})}{r_{sh}} \right\}$, which implies that FF increases with the increase of V_{OC} that varied depending on illumination as well. However, continuously increasing the light intensity leads to non-negligible value of r_s so that decreases FF value. Hou's group [21] explained the phenomenon of the bell shape of FF value versus illumination. The carrier density is high under the strong illumination; thus, bimolecular recombination is the main way of carrier recombination. FF will increase when the illumination reduces, as bimolecular recombination is mitigated in the circumstance of declination of light intensity. However, if illumination continually decreases until carrier density declines to a certain value, the trap-assisted recombination becomes dominate factor so that FF decreases. Therefore, suppressing trap-assisted plays an important role in achieving high FF value under dim light. Decreasing the density of trap state via effective phase-separation control and the increment of domain purity. Through employing highly crystalline active material, adjusting the interfacial ingredient ratio of donor and acceptor, electrode interlayer, and/or adopting the ternary blend system, the morphology near the interface can be optimized to decrease the trap state density [59]. Kwon [60] stated that larger phase separation can mitigate interfaces of active layer so that contribute to more compact film and smaller leakage currents.

3. IOPVs performance characterization and implication

3.1. The description of lighting intensity

It should be noted that the lighting intensity of AM1.5 is represented with radiometric units of W m^{-2} or mW cm^{-2} . Outdoor 1-sun illumination which simulates the intensity of AM1.5 is 100 mW cm^{-2} . Whereas, the indoor lighting intensity is expressed in photometric units of lumens or lux, which is correlative with the spectral luminous efficiency of human eyes versus visible light wavelength. The illumination intensity of indoor conditions are 2 orders of magnitude less than AM1.5. The intensity of 1 sun approximately equals to $100\,000 \text{ lux}$ [10, 15,61]. Although directly comparing the energy emission between the sun and the artificial lights is meaningless due to their different spectra, it is easy to understand the relationship of the magnitudes. The illumination intensities adopted to test indoor photovoltaic cells are frequently under 200, 500 and 1000 lux, respectively, for most of the recent studies. These illumination intensities represent the illumination requirement for different indoor places. For example, 200 lux is used for living rooms and corridors; 500 lux is recommended for offices and classrooms; 1000 lux is suitable for supermarkets and operating rooms.

Chen et.al indicated that the sensitivity of human eyes varies with wavelength distributed over the visible spectrum [62]. In other words, the efficiency that produces a visual response of different wavelengths is defined as luminous efficiency of human eyes. For measuring the photometry based on a uniform standard, the International Commission on Illumination created the spectral luminous efficiency curves which are shown in Fig. 4. There are two situations, one is light-adapted condition (the “photopic” or $V(\lambda)$ function), and the other one is a dark-adapted condition (the “scotopic” or $V'(\lambda)$ function). The photopic condition $V(\lambda)$ described as good lighting conditions is used for almost all the measurements. The illuminance intensity (E_V) (unit: lux) is derived from the emission spectrum collected from spectrometer and $V(\lambda)$, which is displayed in Eq. (10).

3.2. Accurate photoelectric parameter measurement

Capability of devices that converts incident light power into electrical power is evaluated by PCE. $PCE = P_{out}/P_{in} \times 100\%$ (where P_{out} is output power density and P_{in} is incident power density). $P_{out} = V_{OC} \times J_{SC} \times FF$ and P_{in} should be accurately measured. The $J-V$ measurement signals are recorded by a source-measure unit, and values of V_{OC} , J_{SC} , FF , and PCE are collected. Therefore, photoelectric properties under AM1.5 and different indoor lighting sources for photovoltaics are measured and compared, followed by further studying the deeper reasons of their performance by determining the dependency of J_{sc} and V_{OC} on light intensity varied from 100 mW cm^{-2} to 0.1 mW cm^{-2} . If the slope of J_{sc} is close to 1, the bimolecular recombination is weak. If the slope of V_{OC} is close to KT/q , it implies that the bimolecular recombination is sole [63]. Subsequently, whether the trap-assisted recombination is serious that can be deduced.

The fixed illuminance intensity used to supply solar energy is calibrated by the certified standard silicon solar cell. Unlike solar simulator, there is no specified indoor lighting source and no uniform standard for testing the IOPVs. To precisely measure the PCEs of an IOPV harvesting energy from a non-standard illumination condition, the incident light intensity should be accurately evaluated at each time. Hence wavelength resolved spectra of different indoor light sources are measured with a calibrated spectrometer. A spectrometer with an optical fiber used to measure the absolute emission power spectrum is equipped with a cosine corrector. Cosine correctors are optical diffusers on the end of fibers to collect signal from 180° field of view. Both the illumination intensity (unit: lux) and P_{in} (unit: mW cm^{-2}) of the different indoor lighting sources (e.g. LED, Fluorescent, halogen) with various color

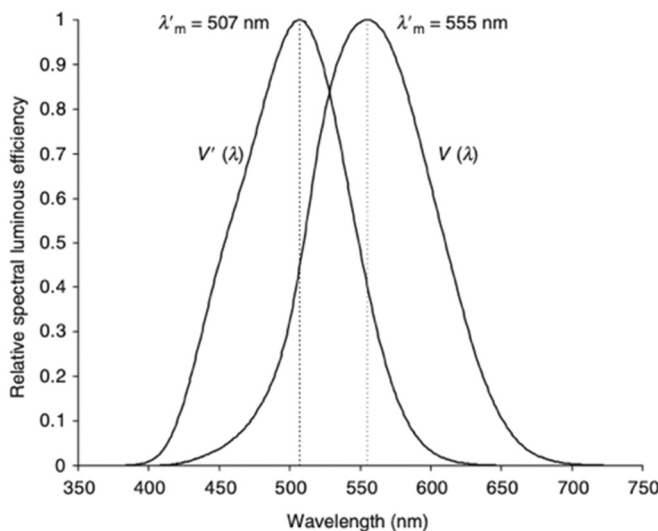


Fig. 4. Commission International de l'Eclairage (CIE) photopic and scotopic luminous efficiency functions $V(\lambda)$ and $V'(\lambda)$ [62]. Copyright 2012, Springer.

rendering (e.g. warm white: 2700 K; cold white: 6500 K) can be integrated from the emission power spectrum (unit: $\mu\text{W cm}^{-2} \text{ nm}^{-1}$) measured from the spectrometer. In the following, photon flux spectrum $N_\lambda(\lambda)$ (unit: $\text{n s}^{-1} \text{ cm}^{-2} \text{ nm}^{-1}$) is calculated from light power spectrum E_λ (unit: $\mu\text{W cm}^{-2} \text{ nm}^{-1}$). The detail Eq. is shown:

$$N_\lambda(\lambda) = E_\lambda \cdot e \cdot \lambda / hc \quad (8)$$

Where e is the elementary charge, λ is the wavelength, h corresponds to the Planck constant and c is the lightspeed. Subsequently, the incident theoretical integral current density (unit: $\mu\text{A cm}^{-2}$) can be integrated by the following Eq.:

$$J = \int_0^\infty N_\lambda(\lambda) d_\lambda \cdot e \quad (9)$$

The illuminance intensity (E_V) can be integrated by the following Eq.:

$$E_V = K_m \int_0^\infty E_\lambda(\lambda) \cdot V(\lambda) d_\lambda \quad (10)$$

Where the coefficient K_m equals 683 lm/W, and E_λ represents emission spectrum. $V(\lambda)$ as described in Fig. 4 is luminous efficiency functions for human eyes. Based on the EQE curve and normalized emission power curve, the short circuit current J_{sc} can be calculated from incident integral current density J by the following Eq.:

$$J_{sc} = \int_0^\infty N_\lambda(\lambda) \cdot EQE(\lambda) d_\lambda \cdot e \quad (11)$$

It should be noted that a low precise lux meter used to measure indoor illuminance conditions will lead to great error. Also, the calculated current based on the combination of EQE curve and photon flux spectrum cannot be acquired to prove the accuracy of the measurement results. Furthermore, the spherical probes installed for lux meters are not suitable for metering the incident emission power of the planar IOPVs [39]. Hence, an enlarged PCE is evaluated ascribed to big errors.

For instance, an overestimated PCE was obtained under 1000-lux illumination tested by a lux meter [64]. The verification work of overestimated PCE was demonstrated by Hou's group [39]. Under the 1000-lux illumination measured by a lux meter rather than a spectrometer, the J_{sc} of device measured from $J-V$ data is $133.1 \mu\text{A cm}^{-2}$ with the calculated incident power (P_{in}) of $278 \mu\text{W cm}^{-2}$. Based on the EQE curve as shown in Fig. 5(a) and the normalized emission power curve displayed in Fig. 5(b), the photon flux spectrum (Fig. 5(c)) corresponding the measured current density is inverse deduced by Eq. 11. Next, the maximum theoretical integral current of incident light converted from the photon flux spectrum is calculated as $183.1 \mu\text{A cm}^{-2}$. Subsequently, the emission power illustrated in Fig. 5(d) of the lighting source is obtained. The integral power spectrum is further transformed, and the integrated power is $401.1 \mu\text{W cm}^{-2}$ (1607 lux). Hence, based on $PCE = P_{out} / P_{in}$, the real P_{in} is higher than lux meter measured power, which leads to the exaggerated PCE. In other words, lux meter is too rough to confirm incident power and results in imprecise PCE. Besides, Hou's group also mentioned that the power distribution of indoor light decays outward from the center which gives rise to have inhomogeneous light power distribution [21]. Therefore, the tested devices should be placed near the center under the light source.

3.3. The effect of R_s and R_{sh} on PCE under low illumination

According to the Shockley Eq., J_{SC} can be expressed as:

$$J_{SC} = \frac{1}{1 + R_s/R_{sh}} \left[J_{ph} - J_0 \left\{ \exp \left(\frac{|J_{SC}|R_s A}{nKT/q} \right) - 1 \right\} \right] \quad (12)$$

Where R_s is series resistance, R_{sh} is shunt resistance to which the leakage current is related, is photo-generated current and J_0 is reverse saturation

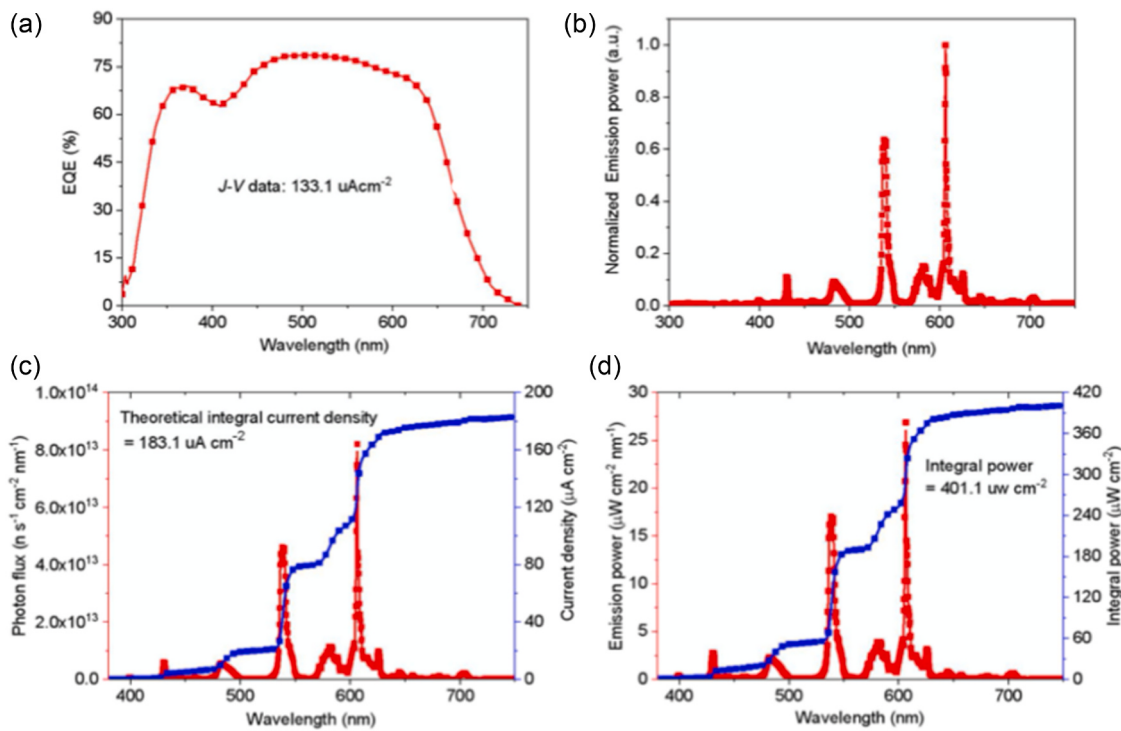


Fig. 5. (a) The EQE curve and (b) the normalized emission spectrum under the 1000-lux fluorescent lamp in the example reference [64]. Copyright 2018, Royal society of chemistry. (c) Derived photo flux and integral current density spectra of incident illumination. (d) Converted emission power and integrated power spectra of incident illumination [39]. Copyright 2019, Nature energy.

current density. Corresponding to Eq. (12), the large $R_s A$ results in small J_{SC} under solar irradiation. However, when light sources are switched from AM1.5 to indoor illuminance, the section $\exp\left(\frac{|J_{SC}|R_s A}{nKT/q}\right) - 1$ is negligible as the J_{SC} dramatically decreases to the level that is much lower than the thermal voltage nKT/q , even multiplied by a large $R_s A$. Nevertheless, a large R_{sh} is not only essential to maintain high V_{OC} but

also to decrease R_s/R_{sh} so that high J_{SC} and PCE can be achieved. The reverse current in the dark is related to the leakage current which can be measured by $J-V$ measurement in dark. Due to small J_{SC} under dim light environment, the increased R_s that arises from large area fabrication and/or adopting cost-effective PEDOT: PSS (pH1000) to replace high-cost ITO electrodes will not significantly affect the devices photoelectric properties. Hence, OPV cells under indoor condition is suitable for

Table 1
Fullerene-based IOPV performance under dim light conditions.

Active layer	Light source	Illumination (lux)	PCE (%)	V_{OC} (V)	J_{SC} (mA cm^{-2})	FF (%)	P_{out} ($\mu\text{W cm}^{-2}$)	Ref.
P3HT: ICBA*	FL	500 ^a	13.76	0.73	0.05	62	22.57	[11]
P3HT: PC ₆₁ BM*	FL	500 ^a	9.59	0.43	0.062	59	15.77	[11]
PTB7-Th: PC ₇₁ BM*	FL	500 ^a	13.14	0.58	0.063	59	21.56	[11]
PTB7-Th: PC ₇₁ BM (1 cm^2)	LED	890 ^b	11.63	0.62	0.092	74	42.3	[78]
PTB7: PC ₇₁ BM (0.15 cm^2)	LED	500*	9.11	0.6	0.046	54.3	15.487	[79]
BTR: PC ₇₁ BM (0.15 cm^2)	FL	1000 ^a	28.1	0.791	0.133	75.2	78.2	[64]
PDTBTBz-2 F _{anti} : PC ₇₁ BM (0.1 cm^2)	LED	1000*	23.1	0.817	0.1124	70.4	64.68	[22]
P3HT: PC ₇₁ BM (0.1 cm^2)	LED	1000*	9.4	0.498	0.0737	71.9	26.32	[22]
PBDB-T: PC ₇₁ BM (0.1 cm^2)	LED	1000*	15.3	0.669	0.0902	71.3	42.84	[22]
PCDTBT: PC ₇₁ BM (0.1 cm^2)	FL	300 ^a	16.6	0.41	0.0277	69.3	17.08	[56]
PCDTBT: PC ₇₁ BM (0.1089 cm^2)	LED	300*	18.72	0.737	0.0311	63.4	14.53	[65]
P1: PC ₇₁ BM (0.1089 cm^2)	LED 3000 k	300*	19.15	0.758	0.02956	66.1	14.86	[65]
PM6: PC ₇₁ BM (1 cm^2)	LED	1000 ^b	18.1	0.784	0.0941	67.1	54.69	[80]
PPDT2FBT:PC ₇₁ BM (0.1 cm^2)	LED	1000*	16	0.587	0.117	65.2	44.8	[68]
PPDT2FBT:PC ₆₁ BM (0.09 cm^2)	LED	1000 ^b	11.8	0.62	0.085	69.5	36.7	[76]
PV2001: PC ₆₁ BM (module:13.6 cm^2)	FL	1000 ^a	13.4	4.81	0.104	60	37.734	[77]
PV2001: PC ₆₁ BM (module:13.6 cm^2)	LED	1000 ^a	13.0	4.89	0.124	61	46.199	[77]
WF3:PC ₇₁ BM (0.15 cm^2)	LED	500*	12.83	0.58	0.06	65.5	21.811	[67]
WF3S:PC ₇₁ BM (0.15 cm^2)	LED	500*	14.32	0.63	0.062	66.9	24.344	[67]
WF3F:PC ₇₁ BM (0.15 cm^2)	LED	500*	17.34	0.7	0.065	69	29.478	[67]
BDT-2 T-ID: PNP (0.06 cm^2)	LED 2900k	200 ^b	16.2	0.75	0.0246	69	12.4	[75]
BDT-2 T-ID: PNP (module:9.5 cm^2)	LED 2900k	200 ^b	15.25	4.2	0.0399	66	11.68	[75]
PTB7: PNP (0.06 cm^2)	LED	200 ^b	9.9	0.58	0.0193	68	7.6	[75]

* There is no description about area of cells and/or the measurement for illumination and incident emission power.

^a Lux meter is used to measure indoor lumen; rough light power is calculated from lux meter or measure by Si detector or rough power meter.

^b Spectrometer/spectrodiometer is used to measure indoor intensity; lux meter is used to measure lumen.

commercialization owing to large surface processability and low-cost superiority [22,52,56].

Briefly, the desired PCE can be obtained owing to matching absorption spectrum, low V_{OC} loss, high EQE response, relatively low trap recombination, and extremely high shunt resistance with low leakage current.

4. Recent indoor organic photovoltaics progress

4.1. Fullerene acceptors

Mid bandgap donors blended with wide bandgap fullerene acceptors ($PC_{61}BM$, $PC_{71}BM$, ICBA, PNP) have been reported in the last few years, which produce PCEs ranged from 13% to 28% under artificial lights (Table 1 and Fig. 7). The successful outcomes based on fullerene acceptors arise from the overlapping spectra between active layers and

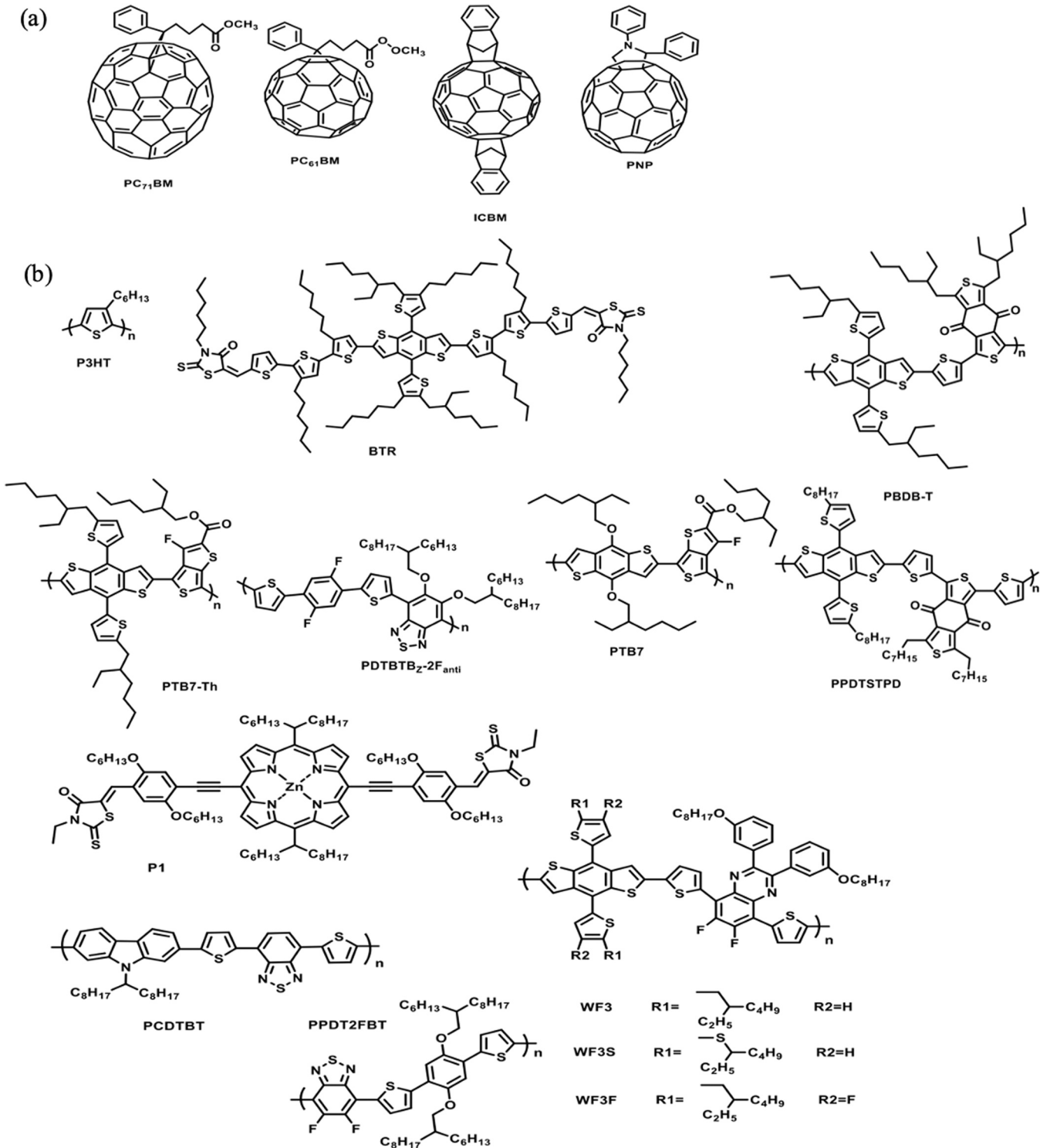


Fig. 7. (a) Chemical structures of fullerene derivatives. (b) Chemical structures of donors applied in fullerene-based devices.

ambient lights. Also, the weak intensities of dim lights compared with AM1.5 avoid causing photodimerization for fullerene and morphology instability [45].

In 2017, different polymer coupled with various fullerene derivatives were investigated, in which P3HT:ICBA achieved best PCEs of 13.76% and 13.05% under 500 lux-illuminance of fluorescent tube and LED lamp, respectively [11]. In comparison with P3HT: ICBA, the systems of P3HT: PC₆₁BM and PTB7-Th: PC₇₁BM produced less PCEs, because of the less energy offsets between the HOMO of polymer donors and LUMO of fullerenes resulting in lower V_{OC} (Fig. 6(a)). Hence, the performance of device can be maximized though increasing the energy difference between HOMO of donors and LUMO of acceptors.

Two different donors, P1 and PCDTBT, are adopted to compare their performance under indoor condition. P1 that is an A-D-A structure comprises a porphyrin ring and two ethylrhodanine end groups [65]. Porphyrins has advantages such as low V_{OC} loss and mitigated carrier recombination, which has been successfully applied in dye-sensitized solar cells. In order to demonstrate that lower V_{OC} loss can achieve higher PCE under dim conditions, PCDTBT based BHJ was tested as well. P1: PC₇₁BM based devices showed PCE of 19.2% (V_{OC} changed from 0.896 for AM1.5 to 0.758 for LED) under irradiation of 300-lux LED (3000k), whereas PCDTBT: PC₇₁BM based devices exhibited a lower PCE of 18.72% (V_{OC} changed from 0.923 for AM1.5 to 0.737 for LED). Moreover, in comparison to PCDTBT, porphyrin based BHJ showed thickness independence ascribed to low electronic disorders.

The impact of solvent vapor annealing (SVA) time was investigated by Tsoi et al. [64]. The system BTR: PC₇₁BM annealed by tetrahydrofuran with 2–5 min achieved the optimal PCE of 28.1%. The optimal SVA treatment time could achieve the appropriate film morphology in which the growing crystallization and the enlarged phase separation were balanced. They demonstrated that V_{max}/V_{OC} (V_{max} is the voltage at the maximum power point) was stable as shown in Fig. 6(b), when the light intensities of sun varied from 1 to 0.1, which indicated that the fractional-voltage method was suitable to track the maximum power points (MPPs) of the low power consumption applications. Furthermore, Yu's group [66] illustrated that BTR dissolved in non-halogenated solvents exhibits high efficiency, which can be coated on substrates by the large-scale-print technology of slot-die coating.

In 2019, Shim's group [22] investigated the performance of BDT based wide bandgap donor PDTBTBz-2 F_{anti} with fullerene acceptor PC₇₁BM under artificial lighting conditions, in comparison with other donors which are P3HT, PBDB-T, PTB7, respectively. The PCE of 23.1% under 1000-lux of LED exceeded that of Si-based IPVs (16.3%). The good photoelectric performance under indoor condition was ascribed to low leakage current, matching spectrum, deeper HOMO leading to larger V_{OC} (0.817 V). The finite-difference time-domain (FDTD) method was

adopted to simulate the power absorption ratios for different devices in order to study the importance of spectrum match between the lighting sources and active layers. They suggested the spectrum match ratio was consistent with J_{SC} . Owing to the optimal power absorption ratio of among all the studied devices, the J_{SC} of PDTBTBz-2F_{anti}-based cells was highest which agreed with the best PCE. Shim's group revealed that the work function (5.5 eV) of PDTBTBz-2F_{anti} was slightly deeper than that of holes transporting layer PEDOT: PSS (5.2 eV) which could induce the depletion of holes, thus lead to bigger V_{OC} loss under 1 sun illuminance. However, due to the lower carrier densities under dim light conditions, the quasi-fermi level of PDTBTBz-2F_{anti} became shallower than PEDOT: PSS and could be in charge of the minimum V_{OC} loss (9%) when switched light sources compared with other donors mixed with PC₇₁BM (P3HT:20%, PBDB-T:12%, PTB7:11%). The research indicated that the influence of R_s in FF was negligible under dim light conditions. On the contrary, R_{sh} played an important role in determining FF, which was revealed through analyzing the semi-empirical Eq. of FF.

Lee's group [67] designed and synthesized a series of D-A structure polymer donors comprising BDT moiety and 5,8-bis(5-bromothiophen-2-yl)-6,7-difluoro-2,3-bis(3-(octyloxy)phenyl)quinoxaline with different thienyl substitution on the part of BDT. The results demonstrated that, in comparison with alkyl (WF3) and alkylthio substituents (WF3S), F substituent (WF3F) can minimize bimolecular recombination, reduce R_s , increase R_{sh} , suppress trap-assisted recombination, higher V_{OC} , and better morphology. Hence, under 500-lux LED condition, WF3F: PC₇₁BM with diphenyl ether as an additive presented PCE of 17.34% which surpassed that of WF3 with 12.83% and WF3S with 14.32%. This work verified that through finely tuning the polymer molecular structure, the photoelectrical properties of polymer based OPVs can be effectively improved.

In order to study the influence of thickness of active layers on PCE under weak illuminations, the thickness of PPDT2FBT:PC₇₁BM-based photoactive layer was increased from 170 nm to 760 nm under intensity of 1000 lux, PCEs locate between 13% and 16% with thickness tolerant J_{sc} and FF values [68], where the optimal thickness was 390 nm. In comparison with exact thickness processed by spin coating in lab, the thickness in large-scale production is less accurate, therefore, a certain thickness tolerance property of IOPVs is desirable [6,69–71]. Small's group [72] demonstrated that one of the reasons why the thickness of active layer > 200 nm leading to poor PCE is the accumulation of space charge in the active layer resulting in increased carrier recombination loss [73]. However, when the light intensity dropped from 100 to 11.4 mW cm⁻², the space-charge limited photocurrent with thick active layer of 409 nm decreased because the space charge accumulation is proportional to the light intensity. Woo's group [74] analyzed that the thick active layer is more suitable for IOPVs because a thicker layer may

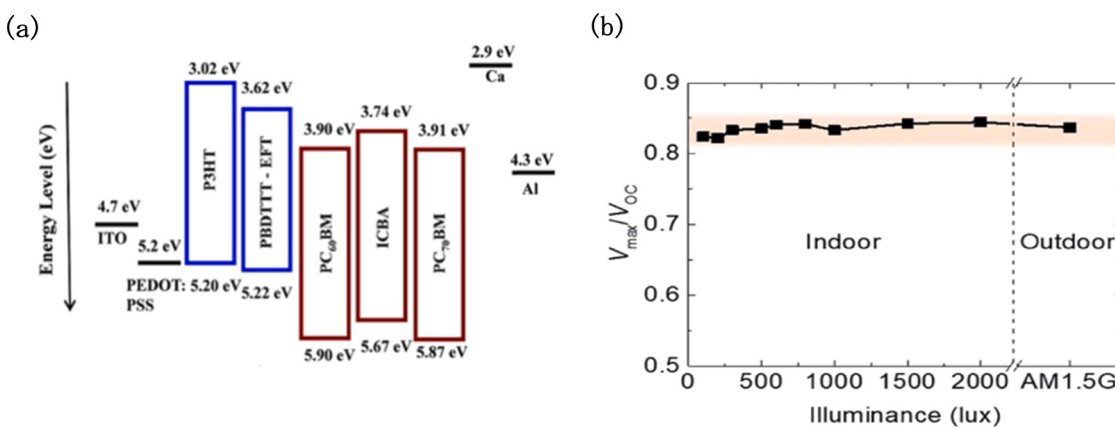


Fig. 6. (a) Energy level schematic of different polymer coupled with various fullerene derivative [11] with permission from John Wiley and Sons (Copyright 2017). (b) The ratios between the voltage at the maximum power point (V_{max}) and the V_{OC} under both indoor and outdoor illuminance [64] with permission from Royal Society of Chemistry (Copyright 2017).

increase R_{sh} to cause a lower leakage current without serious carrier recombination loss. The results of the optimal PCEs with the thickness of 130 nm under AM1.5 and the thickness of 230 nm under dim light, for PPDT2FBT:PC₇₁BM-based photoactive layer, support Woo's assumption.

A small molecules BDT-2T-1D and an analogous polymer PTB7 were mixed with a fullerene acceptor PNP [75]. As BDT-2T-1D has deeper HOMO, its V_{OC} is higher than PTB7-based device leading to better PCE of

16.2% than that of PTB7-based device (PCE=9.9%), under 200-lux LED illumination. Moreover, both rigid glass and flexible polyethylene naphthalate (PEN) were adopted as substrates for fabricating large area IOPV modules. Over PCE of 15% was achieved for both rigid and flexible modules constructed by six sub cells in series, producing power over 100 μ W with a high V_{OC} of 4.2 V.

The polymer donor PPDT2FBT blended with PC₆₁BM, ITIC-M, ITIC-F, and tPDI₂N-EH, respectively, dissolved in green halogenated-free

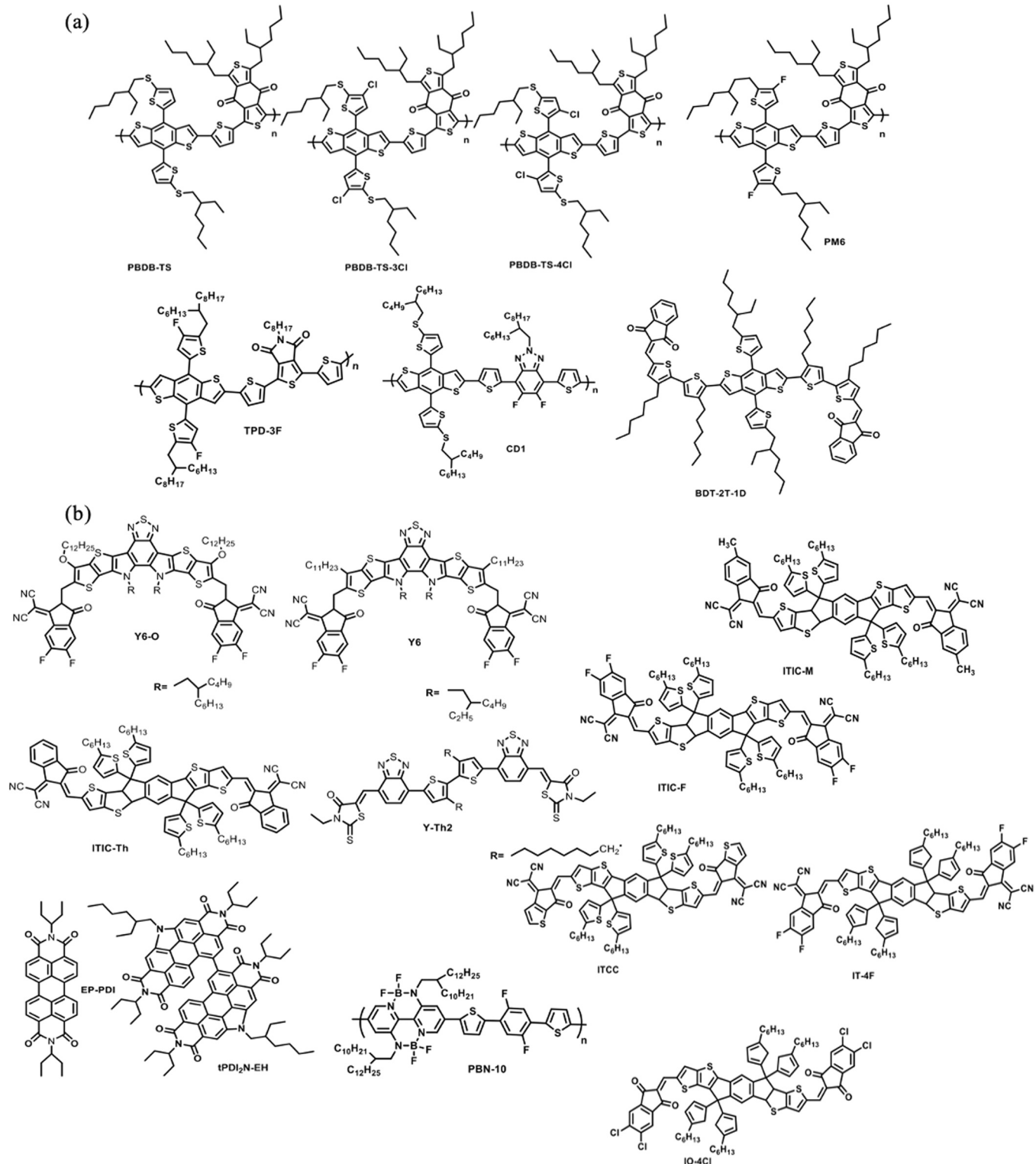


Fig. 8. Chemical structures of (a) donors and (b) acceptors adopted in non-fullerene based IOPV devices.

solvent followed by slot-die coating onto substrates [76]. Among the devices, fullerene based IOPVs exhibited best PCE of 11.8% under 1000 lux LED illumination. In 2020, Vilkman et al. [77] studied the performance of 13.6 cm² modules with 8 cells in series in the flexible architecture of PET/ ITO/ SnO₂/ PV2001: PC₆₁BM/ PEDOT: PSS/ silver grid under LED and FL conditions. SnO₂ as electron transporting layers and active material in the blend solution were slot-die coated with a roll to roll process into the flexible substrate. In the following, the grid silver as hole transporting layers was printed on substrate which was cut into sheet to sheet. The large area module exhibited PCEs over 13.4% with P_{out} of 513.2 μW and 13% with P_{out} of 628.3 μW, under FL and LED illumination, respectively, which verified that SnO₂ was a substitute material for ZnO for indoor applications. Moreover, the authors stated that, under same lux level, LED has higher emission power than FL, leading to lower PCE but higher P_{out} .

4.2. Non-fullerene acceptors

The fullerenes located at the UV-vis region made the blend film's absorption spectrum match well with the LED and FL emission spectra, but the relatively deeper LUMO of fullerenes cause larger V_{OC} loss and low absorbance in visible spectrum resulted in relatively lower J_{SC} . Moreover, the non-tunability of energy level of fullerene derivatives makes photoelectric performance hardly improved. Therefore, non-fullerene acceptors are explored for IOPVs (Fig. 8).

Kwon and coworkers [60] in 2019 demonstrated the effect of chlorination of PBDB-TS (Table 2). The polymer donors of PBDB-TS, PBDB-TS-3Cl, PBDB-TS-4Cl which have the core of BDT-Th were coupled with donor ITIC, respectively. Under outdoor condition, chlorination didn't exhibit perceptible effect on the performance. However,

under fluorescent lamp, the best PCE of 21.7% was achieved by PDBD-TS-4Cl based devices, followed by the PCE of PDBD-TF-3Cl based devices (20.4%) and the quite low PCE of non-chlorination PBDB-TS based devices (5.2%). Kwon summarized that the performance improvement of chlorination of the polymer under artificial lamps was owing to efficient harvesting for fewer photons, the better morphology with better charge mobility, lower leakage current, and smaller V_{OC} loss.

In 2019, Hou's group [80] fabricated 1 cm² PM6: ITCC, PM6: IT-4F, PM6: PC₇₁BM devices, respectively, to verify the possibility of large-area processability. ITCC-based device achieved 1.1 V and 0.962 V under illuminance of 1-sun and 1000 lux-LED, respectively, compared with PC₇₁BM-based device of 0.945 V and 0.784 V, and IT-4 F-based devices of 0.872 V and 0.712 V. The PCE 22% of ITCC based devices surpassed that of PC₇₁BM-based devices (18.1%) and IT-4F-based devices (20.8%) under 1000 lux LED (2700k). Although the trap-assisted recombination became more and more serious with decreasing the solar intensities from 100 mW cm⁻² to 0.1 mW cm⁻², the trap-mediated charge recombination of ITCC-based was minor than that of PC₇₁BM-based and IT-4F-based under weak illumination, leading to better performance. They also revealed that illumination and heat were the main reasons for PCE decline of IPV cells. In contrast to strong illumination, the devices showed much greater stability under continuous dim light illumination. Moreover, Hou verified that if the lux meter was used to measure the indoor lighting intensities, a large error would be caused. The input power of illumination should be accurately measured by the spectrometer to correctly evaluate the performance of devices.

Hou's group [39] further synthesized a new wide bandgap non-fullerene acceptor IO-4Cl blended with PM6 which achieved 26.1% PCE and a literally large V_{OC} of 1.1 V under 1000 lux of LED (2700k). The structure of A-D-A was commonly adopted in non-fullerene

Table 2
Non-fullerene based IOPV performance under dim light conditions.

Active layer	Light source	Illumination (lux)	PCE (%)	V_{OC} (V)	J_{SC} (mA cm ⁻²)	FF (%)	P_{out} (μW cm ⁻²)	Ref.
PM6: Y6-O (0.08 cm ²)	LED 3000k	1650 ^b	30.89	0.84	0.245	77	161.23	[37]
PM6: ITCC (1 cm ²)	LED 2700k	1000 ^b	22	0.962	0.095	64.3	66.48	[80]
PM6: IT-4 F (1 cm ²)	LED 2700k	1000 ^b	20.8	0.712	0.113	68.7	62.86	[80]
PBDB-TS:IT-4F (0.0422 cm ²)	FL	500 ^a	5.3	0.36	0.0668	63.3	22.1	[60]
PBDB-TS-3Cl:IT-4F (0.0422 cm ²)	FL	500 ^a	20.4	0.64	0.0628	73.7	60.2	[60]
PBDB-TS-4Cl:IT-4F (0.0422 cm ²)	FL	500 ^a	21.7	0.64	0.0649	70.2	64	[60]
PM6: IO-4Cl (1 cm ²)	LED 2700k	1000 ^b	26.01	1.10	0.09	79.1	78.8	[39]
PM6: IO-4Cl (4 cm ²)	LED 2700k	1000 ^b	23.9	1.07	0.089	75.3	72.1	[39]
CD1: PBN-10 (0.08 cm ²)	FL	1000 ^a	26.2	1.14	0.120	66.2	91	[87]
CD1: PBN-10 (0.08 cm ²)	LED	1000 ^a	21.7	1.14	0.105	65.4	78	[87]
CD1: ITIC (0.08 cm ²)	FL	1000 ^a	8.69	0.78	0.116	68.1	62	[87]
CD1: ITIC (0.08 cm ²)	LED	1000 ^a	17.9	0.77	0.107	67.5	56	[87]
TPD-3 F: IT-4F (5.95 cm ²)	FL	1000 ^b	26.2	0.75	3.98	65.1	48.5	[88]
TPD-3 F: IT-4F (module:20.4 cm ²)	FL	1000 ^b	21.8	3.21	0.361	70.6	40.2	[88]
PPDT2FBT: ITIC-M (0.09 cm ²)	LED 5600k	1000 ^b	7.5	0.62	0.0685	54.6	23.2	[76]
PPDT2FBT: ITIC-F (0.09 cm ²)	LED 5600k	1000 ^b	4.7	0.45	0.0855	37.6	14.5	[76]
PPDT2FBT:tPDI ₂ N-EH (0.09 cm ²)	LED 5600k	1000 ^b	8.9	0.84	0.0654	50.2	27.6	[76]

^a There is no description about area of cells and/or the measurement for illumination and incident emission power.

^b Lux meter is used to measure indoor lumen; rough light power is calculated from lux meter or measure by Si detector or rough power meter.

^b Spectrometer/spectrodiometer is used to measure indoor intensity; lumen is calculated from light intensity or measured by lux meter.

acceptors [81–86]. This device possessed remarkable stability. IO-4Cl ranged from 450 to 700 nm with a wide optical bandgap of 1.8 eV. Through investigating the reason of high V_{OC} , a radiative recombination above the gap ΔE_1 of ca. 0.28 eV, a radiative recombination below the gap ΔE_2 of ca. 0.07 eV, and a non-radiative recombination ΔE_3 of ca. 0.25 eV were measured. Both low ΔE_2 and ΔE_3 contributed a relatively small V_{OC} loss. In order to prove the large-area processability for IOPVs, even 4 cm² devices through the blade-coating process showed 23.9% PCE with a thicker active layer. As shown in Fig. 9(a), by increasing the external additional series resistor, the devices performance under AM1.5 and 500 lux-LED were observed. In comparison with almost constant PCEs under weak illumination, the photoelectric performances under outdoor condition decreased, as mentioned before, which implies that IOPVs are insensitive to series resistance. Also, the devices showed remarkable stability under continuous illumination over 1000 h (Fig. 9(b)), which demonstrated that the gentle light intensity can better maintain the stability of cells.

Besides star polymer donor PM6, a medium bandgap polymer donor CD1 [87] mixed with PBN-10 and ITIC was studied to fabricate

all-polymer cells. Thanks to aligned energy level of donor and acceptor, CD1: PBN-10 blend acquired a quite high V_{OC} of 1.14 resulting in PCEs of 26.2% and 21.7% under illuminance of FL and LED, respectively. Due to the larger LUMO offset between CD1 and ITIC resulting in smaller V_{OC} , CD1: ITIC blend showed PCEs of 17.9% and 15.4% under FL and LED, respectively.

Yan et al. [37] in 2020 focused on the influence of electron transporting layers on the IOPVs under weak illumination. An acceptor Y6-O was blended with PM6 which was applied with different electron transporting layers, PDINO (HOMO: -6.21 eV) and PFN (HOMO: -5.61 eV), respectively. The work functions of cathode electrode Al applied different interlayers were measured by ultraviolet photoelectron spectroscopy (UPS). As shown in Fig. 9(c), the work function (WF) downshifted from 4.22 to 3.97 eV when applied with PDINO on Al, and WF shifted from 4.22 to 4.12 eV when applied with PFN. Although both interlayers could reduce the WF of cathode Al to improve electrons extraction, the Δh , the difference between the HOMO of the interlayer and the fermi level of the cathode, which expressed the hole blocking barrier, were different. The PDINO based devices with the Δh of 2.31 eV

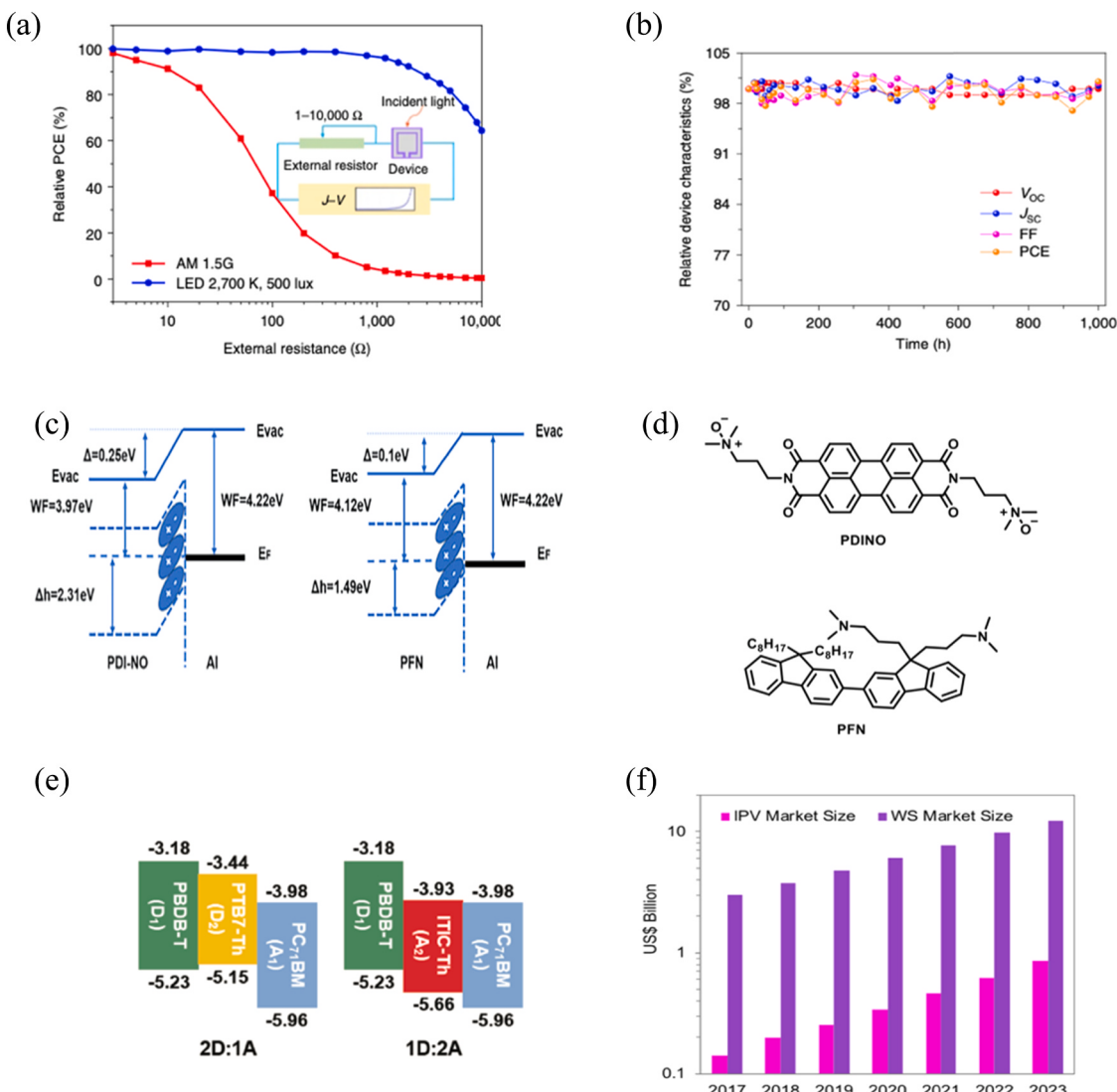


Fig. 9. (a) Photovoltaic performance varying with the external resistance under AM1.5 and 500 lux-LED, respectively [39]. (b) Compared with initial photovoltaic performance, dependence of relative device characteristics on time under continuous illumination with the temperature of 25–30 °C and humidity of 40%–60% [39]. Copyright 2019, Nature. (c) The energy level outline of PDINO, PFN and Al [37] with permission from Elsevier (Copyright 2020). (d) The molecular structures of electron transport layers of PDINO and PFN. (e) Energy levels of D1:D2: A and D: A1:A2 models incorporating the third component PTB7-Th as D2 or ITIC-Th as A2 in PBDB-T [96] with permission from John Wiley and Sons (Copyright 2019). (f) The predicted market size of IPV and WS [14] with permission from Elsevier (Copyright 2019).

was larger than that of PFN based devices (1.49 eV), which indicated that the hole blocking ability of PDINO was better. The photoelectric properties of two types of interlayers' cells were similar under AM1.5, whereas PCE of PDINO-based was 30.02% and PCE of PFN-based was 22.47% under 1650-lux LED (3000 k). Yan's group speculated that the worse trap-assisted recombination occurred in PFN based devices with low carrier density under weak light intensities due to the smaller Δh compared with the PDINO based devices. However, the influence of these two interlayers could be negligible under strong light intensities because of their high carrier density.

To accelerate the commercialization process, a large area individual cell of 5.95 cm^2 and module with 5 cells in series of 20.4 cm^2 (maximum value to date) were fabricated by active layer of TPD-3F: IT-4F. The P_{out} of cell and module realized $48.5\text{ }\mu\text{W/cm}^2$ and $40.2\text{ }\mu\text{W/cm}^2$, with PCE of 26.2% and 21.8%, based on the irradiation of 1000 lux FL, respectively [88]. The polymer donor TPD-3F consisted a BDT donor moiety and 2, 5-dithienyl-thieno[3,4-c]pyrrole-4,6-dione acceptor moiety, which was readily dissolved in halogenated-free solvent. The photovoltaic properties of this blend were insensitive to blade coating compared with spin coating, solvent, and polymer molecular mass.

4.3. Ternary strategy

Ternary bulk heterojunction (BHJ) approaches have been testified as a useful way to further enhance the performance of OPVs in both outdoor and indoor environments. The ternary strategy summarized in Table 3 includes two structures which are D1:D2:A (two donors and one acceptor) and D:A1:A2 (one donor and two acceptors), where the extra third component can broaden the photon utilization of the emission spectrum, promote charge transport, improve BHJ morphology, and prevent active layer degradation [89–93]. Similarly, quaternary structure can also improve.

The ternary strategy was applied to improve the performance of IOPVs by So' group [19]. PDTSTPD as the ternary composition was doped into PCDTBT: PC₇₁BM resulting in the PCE improvement increased from 16.5% to 20.8% under the 300-lux fluorescent lamp (2700 k). The ternary device showed improved hole mobility and passivated shallow traps ascribed to dope with the third component. In contrast to binary devices, ternary devices had higher V_{OC} of 0.89 V under 1-sun illuminance, while 0.73 V under dim light irradiance was achieved. Ternary-based cells had higher J_{SC} than binary-based cells owed to the complementary absorption spectrum of the third component to better utilize the emission of indoor tube. Moreover, the ternary films showed narrower band tail and improved hole mobilities, indicating shallow traps near the band edges are mitigated [94,95].

Ko et al. [96] investigated D1:D2: A and D:A1:A2 models, which were PBDB-T:PTB7-Th: PC₇₁BM and PBDB-T:ITIC-Th: PC₇₁BM (Fig. 9 (e)), yielding PCE of 20.12% ($V_{\text{OC}} = 0.63\text{ V}$, $J_{\text{SC}} = 159.99\text{ }\mu\text{A cm}^{-2}$, and $FF = 65.06\%$) and 26.4% ($V_{\text{OC}} = 0.72\text{ V}$, $J_{\text{SC}} = 157.94\text{ }\mu\text{A cm}^{-2}$, and $FF = 54.43\%$) under 1000-lux LED, respectively. The result showed that both approaches improved performances of cells when referenced to binary blend with PCE of 15.23% ($V_{\text{OC}} = 0.61\text{ V}$, $J_{\text{SC}} = 140.15\text{ }\mu\text{A cm}^{-2}$, and $FF = 49.6\%$). The result implied that the third non-fullerene acceptor, ITIC-Th, self-organized at the interface of polymer: fullerene,

forming cascade ternary junction can result in less charge recombination, higher V_{OC} and PCE compared with binary blend [97]. However, in comparison with D:A1:A2, additional donor, PTB7-Th failed in forming self-optimized ternary junction formation, suffering relatively severe charge recombination. The authors concluded that the third component should be compatible with the host materials and preferably emerge at interfaces of donor and acceptor in order to form cascade energy levels.

Similarly, the strategy of multiple acceptors coupled with one donor was applied by Lee's group [79]. EP-PDI was doped into the mixture of PTB7: PC₇₁BM. The ratio of 40%:60% for EP-PDI: PC₇₁BM showed the optimal PCE under both indoor and outdoor conditions which is attributed to the synergistic contribution of improved absorption, enhanced charge transport, and suppressed non-geminate recombination.

A new non-fullerene acceptor, Y-Th2 was designed by Yang's group [98], which has a structure of dual acceptor-donor-dual acceptor (A1:A2-D-A2:A1). Devices made of PM6: Y-Th2:Y6 offers the PCE of over 16% under AM1.5 and achieves the PCE of 22.7% under 1000 lux-LED. The HOMO and LUMO of Y-Th2 aligned between those of binary host, thereby may facilitate efficient carrier transportation due to the cascade energy level. The bandgap of synthesized acceptors was higher than that of donor PM6. Therefore, this acceptor complemented the absorption spectra of PM6 and Y6 in the short wavelength region with a high absorption coefficient to harvest extra photons. Moreover, the result of Grazing-incidence wide-angle X-ray scattering (GIWAXS), exhibited more packed face-on orientation for ternary blend compared with PM6:Y6, which could enhance intermolecular transportation. Transmission electron microscopy (TEM) demonstrated preferential bi-continues interpenetrating network structure after doping 5 wt% Y-Th2. The reported ternary active layer can be applied in both solar cells and indoor light harvesters because of its excellent PCE under outdoor and indoor conditions.

4.4. Molecular design and industrialization perspectives

Leclerc et al. [45] summarized molecular design perspective for high-efficient IOPVs. The bandgap of NFAs should be increased by increasing the electronic density of end group [99–101] or decreasing the backbone planarity [102,103]. Compared with NFAs mixed with donors, fullerene acceptors in devices often exhibit lower V_{OC} due to worse aligned energy levels and larger V_{OC} loss. In order to enlarge V_{OC} , a molecular design strategy of decreasing the electron-withdrawing properties of the A moiety in A-D-A leads to upshift LUMO [104], as demonstrated for IO-4Cl [39]. Also, a downshifting HOMO levels of the donor is necessary.

Although higher intensities usually result in higher PCE, Leclerc [45] stated that lower intensities of 200–500 lux are more practical to evaluate the photoelectric property of indoor energy harvesters because the lower radiances are representative of most indoor conditions. Moreover, in comparison with fluorescent tubes, LED lamps have advantages of a longer mean lifetime, cheaper cost and more efficient energy conservation, which should be as the standardized illuminance light source during measurement.

Mathews et al. [14] provided the technology and market overview for

Table 3
Ternary IOPV performance under dim light conditions.

Active layer	Light source	Illumination (lux)	PCE (%)	V_{OC} (V)	J_{SC} (mA cm^{-2})	FF (%)	P_{out} ($\mu\text{W cm}^{-2}$)	Ref.
PCDTBT: PDTSTPD: PC ₇₁ BM*	FL 3000k	300 ^a	20.8	0.73	0.0333	63.5	15.4	[19]
PBDB-T: PTB7-Th: PC ₇₁ BM (0.114 cm^2)	LED	1000 ^a	18.99	0.63	0.158	53.64	53.173	[96]
PBDB-T: ITIC-Th: PC ₇₁ BM (0.114 cm^2)	LED	1000 ^a	22.73	0.72	0.1559	56.02	63.644	[96]
PM6: Y-Th2:Y6 (0.00477 cm^2)	LED	1000 ^a	22.33	0.701	0.032	74.48	163	[98]
PTB7: PC ₇₁ BM: EP-PDI (0.15 cm^2)	LED	500*	15.68	0.65	0.057	15.36	26.65	[79]

* There is no description about area of cells and/or the measurement for illumination and incident emission power.

^a Lux meter is used to measure indoor lumen; rough light power is calculated from lux meter or measure by Si detector or rough power meter.

IPV cells. A series of low-power consumption protocols that have been realized to fulfill various application of IoT technologies, requires 60 million IPV cells to harvest indoor light sources. Hence, the market (Fig. 9(f)) of IPV cells is predicted to be huge in the near future, and the capital demand of IPVs and wireless sensors (WS) continues to rise to \$ 850 million and \$ 10 billion by 2023, respectively. Mathews predicted that the manufacturing cost of organic IPV cells will range from 0.001 \$ cm⁻² to 0.03 \$ cm⁻² in the next 5 years. Researchers have to pay attention to materials and production in an economical way of ensuring low cost IPV cells at a small-scale production. Furthermore, they mentioned that to developing universally agreed and uniform standards for evaluating IPV cells performance is necessary.

In October 2020, ARMOR solar power films reported that a record 26% efficiency in a 200-lux environment for the ASCA® organic photovoltaic (OPV) cell has been achieved [105]. ARMOR has installed its ASCA® IOPVs at its factories in Kitzingen (Germany) to drive sensors monitoring real time data of ambient temperature and humidity. The collected data that is essential to ensure the quality of production can be accessed remotely for analysis. This report is inspiring for the study of IOPVs.

5. Conclusion and outlook

Numerous low consumptions off-grid applications that connect to the internet emerge recently, the scale of IPVs markets that provide continuous power for indoor conditions is dramatically rising. This review proves that IOPVs technology is a promising candidate to enter the IPVs' market in the near future.

The maximal theoretical PCE of IOPVs under an indoor environment is around 60%, which is much higher than that of Si-based PVs. In order to further improve PCE to near 60%, new wide-bandgap material should be synthesized to better cover emission spectrum of indoor light; trap mediated recombination should be mitigated and V_{OC} loss should be minimized via adopting optimal device structure and process method. Considering capital expenditure of manufacturers, the economical mode to produce IOPVs is essential to ensure low cost for production in small volume. To solve this issue, more cost-effect processes such as slot-die and blade coating are suggested. As performance of IOPVs is not sensitive to R_s , more economical transparent electrode such as PH1000 can be an alternative of ITO. To realize large area producibility in an environment sustainable way, non-halogen solvents such as 1,2,4-trimethylbenzene, tetrahydrofuran and trimethylbenzene are more suitable than chlorobenzene, chloroform, and 1,8-diiodooctane. However, the study about active material well dissolved in green solvents lags behind, which should be attracted more attentions. OPV materials have poor stability under AM1.5 which prevents them from entering the commercial market, despite several outstanding advantages such as their low cost, good flexibility, and transparency. Strong illumination and heat which come from solar irradiation are the two of main reasons that cause OPV cell degradation and OPV performance decays. On the contrary, because of relatively low light intensities, the absence of UV light, and moderate temperature in the indoor environment, cell stability with time is more dependent to film morphology and interface. However, the stability under the condition of oxygen and moisture for IOPVs is rarely studied, and it will be of great significance to be carried out. More study should be focused on the all-polymer IOPVs which exhibit long term air stability. Besides, all-polymer materials show attractive merit in flexible application used in curved surface. Moreover, more research about flexible substrate, top electrode, and interlayer should be carried out. As recent progress about IOPVs summarized above, the light sources, illumination, color temperature, and apparatus that meter the incident emission power have not been uniformed and regulated. In other words, there is no generally accepted standards like solar cells to evaluate the performance of IOPVs. It is not easy to directly compare their efficiency and performance. Hence, it is urgent to develop a standard system to evaluate the photoelectric properties of IOPVs. Moreover, as a higher

PCE may be achieved under a stronger indoor light intensity, a large proportion of work about IOPVs adopted an incident intensity above 1000 lux. However, only commercial venues or hospitals use illuminance above 1000 lux which is not common in most of the buildings, therefore, a lower intensity ranging from 200 to 500 lux recommended for general places is more suitable for the evaluation of IOPVs. Although IOPVs open a new way to harvest indoor energy which can be embedded in a gadget to realize IoT Vision, some critical issues need to be addressed: (a) novel wide bandgap materials with high extinction coefficient should be designed to improve PCE; (b) the development of all-polymer IOPVs which is processable in eco-compatibility solvents with superior air stability should be speeded up;(c) more attention should be given in cost-effective rigid/flexible large scale fabrications with the development of process methods, substrate, electrodes and interlayers; (d) the uniformed criteria to evaluate the performance of IOPVs should be established.

Declaration of Competing Interest

The authors declare that they have no known competing financial interests or personal relationships that could have appeared to influence the work reported in this paper.

Acknowledgments

This work was financially supported by the National Science Fund for Distinguished Young Scholars(21925506), National Key R&D Program of China (2017YFE0106000), National Natural Science Foundation of China (51773212), Ningbo S&T Innovation 2025 Major Special Programme (2018B10055), Ningbo Municipal Science and Technology Innovative Research Team (2015B11002 and 2016B10005), and CAS Key Project of Frontier Science Research (QYZDB-SSW-SYS030).

References

- [1] M.Z. Jacobson, Review of solutions to global warming, air pollution, and energy security, *Energy Environ. Sci.* 2 (2009) 148–173.
- [2] J. Chow, R.J. Kopp, P.R. Portney, Energy resources and global development, *Science* 302 (2003) 1528–1531.
- [3] B.K. Bose, Global warming: energy, environmental pollution, and the impact of power electronics, *IEEE Ind. Electron. Mag.* 4 (2010) 6–17.
- [4] I. Dincer, Renewable energy and sustainable development: a crucial review, *Renew. Sustain. Energy Rev.* 4 (2000) 157–175.
- [5] S. Dai, X. Zhan, Nonfullerene acceptors for semitransparent organic solar cells, *Adv. Energy Mater.* 8 (2018), 1800002.
- [6] R. Søndergaard, M. Hösel, D. Angmo, T.T. Larsen-Olsen, F.C. Krebs, Roll-to-roll fabrication of polymer solar cells, *Mater. Today* 15 (2012) 36–49.
- [7] M. Kaltenbrunner, M.S. White, E.D. Glowacki, T. Sekitani, T. Someya, N. S. Sariciftci, S. Bauer, Ultrathin and lightweight organic solar cells with high flexibility, *Nat. Commun.* 3 (2012) 770.
- [8] C. Sun, R. Xia, H. Shi, H. Yao, X. Liu, J. Hou, F. Huang, H.-L. Yip, Y. Cao, Heat-insulating multifunctional semitransparent polymer solar cells, *Joule* 2 (2018) 1816–1826.
- [9] Q. Liu, Y. Jiang, K. Jin, J. Qin, J. Xu, W. Li, J. Xiong, J. Liu, Z. Xiao, K. Sun, S. Yang, X. Zhang, L. Ding, 18% efficiency organic solar cells, *Sci. Bull.* 65 (2020) 272–275.
- [10] A. Virtuani, E. Lotter, M. Powalla, Influence of the light source on the low-irradiance performance of Cu(In,Ga)Se₂ solar cells, *Sol. Energy Mater. Sol. Cells* 90 (2006) 2141–2149.
- [11] S.-S. Yang, Z.-C. Hsieh, M.L. Keshtov, G.D. Sharma, F.-C. Chen, Toward high-performance polymer photovoltaic devices for low-power indoor applications, *Sol. RRL* 1 (2017), 1700174.
- [12] J.-L. Wu, F.-C. Chen, M.-K. Chuang, K.-S. Tan, Near-infrared laser-driven polymer photovoltaic devices and their biomedical applications, *Energy Environ. Sci.* 4 (2011) 3374–3378.
- [13] G. Denner, S. Bereznev, D. Fichou, K. Holl, D. Ilic, R. Koeppe, M. Krebs, A. Labouret, C. Lungenschmied, A. Marchenko, D. Meissner, E. Mellikov, J. Méot, A. Meyer, T. Meyer, H. Neugebauer, A. Öpik, N.S. Sariciftci, S. Taillemite, T. Wöhrle, A self-rechargeable and flexible polymer solar battery, *Sol. Energy* 81 (2007) 947–957.
- [14] I. Mathews, S.N. Kantareddy, T. Buonassisi, I.M. Peters, Technology and market perspective for indoor photovoltaic cells, *Joule* 3 (2019) 1415–1426.
- [15] F.-C. Chen, Emerging organic and organic/inorganic hybrid photovoltaic devices for specialty applications: low-level-lighting energy conversion and biomedical treatment, *Adv. Opt. Mater.* 7 (2019), 1800662.

- [16] M. Freunek, M. Freunek, L.M. Reindl, Maximum efficiencies of indoor photovoltaic devices, *IEEE J. Photovolt.* 3 (2013) 59–64.
- [17] A. Sacco, L. Rolle, L. Scaltrito, E. Tresso, C.F. Pirri, Characterization of photovoltaic modules for low-power indoor application, *Appl. Energy* 102 (2013) 1295–1302.
- [18] Y. Cui, H. Yao, T. Zhang, L. Hong, B. Gao, K. Xian, J. Qin, J. Hou, 1 cm² organic photovoltaic cells for indoor application with over 20% efficiency, *Adv. Mater.* 31 (2019), 1904512.
- [19] H. Yin, J.K.W. Ho, S.H. Cheung, R.J. Yan, K.L. Chiu, X. Hao, S.K. So, Designing a ternary photovoltaic cell for indoor light harvesting with a power conversion efficiency exceeding 20%, *J. Mater. Chem. A* 6 (2018) 8579–8585.
- [20] C.L. Cutting, M. Bag, D. Venkataraman, Indoor light recycling: a new home for organic photovoltaics, *J. Mater. Chem. C* 4 (2016) 10367–10370.
- [21] Y. Cui, L. Hong, J. Hou, Organic photovoltaic cells for indoor applications: opportunities and challenges, *ACS Appl. Mater. Interfaces* 12 (2020) 38815–38828.
- [22] Y.-J. You, C.E. Song, Q.V. Hoang, Y. Kang, J.S. Goo, D.-H. Ko, J.-J. Lee, W.S. Shin, J.W. Shim, Highly efficient indoor organic photovoltaics with spectrally matched fluorinated phenylene-alkoxybenzothiadiazole-based wide bandgap polymers, *Adv. Funct. Mater.* 29 (2019), 1901171.
- [23] J.F. Randall, J. Jacot, Is AM1.5 applicable in practice? Modelling eight photovoltaic materials with respect to light intensity and two spectra, *Renew. Energy* 28 (2003) 1851–1864.
- [24] J.F. Randall, Designing Indoor Solar Products: Photovoltaic Technologies for AES, John Wiley & Sons, Ltd., 2005.
- [25] M. Freitag, J. Teuscher, Y. Saygili, X. Zhang, F. Giordano, P. Liska, J. Hua, S. M. Zakeeruddin, J.-E. Moser, M. Grätzel, A. Hagfeldt, Dye-sensitized solar cells for efficient power generation under ambient lighting, *Nat. Photonics* 11 (2017) 372–378.
- [26] Y. Cao, Y. Liu, S.M. Zakeeruddin, A. Hagfeldt, M. Grätzel, Direct contact of selective charge extraction layers enables high-efficiency molecular photovoltaics, *Joule* 2 (2018) 1108–1117.
- [27] B. Conings, L. Baeten, T. Jacobs, R. Dera, J. D'haen, J. Manca, H.-G. Boyen, An easy-to-fabricate low-temperature TiO₂ electron collection layer for high efficiency planar heterojunction perovskite solar cells, *APL Mater.* 2 (2014), 081505.
- [28] F. Di Giacomo, V. Zardetto, G. Lucarelli, L. Cinà, A. Di Carlo, M. Creatore, T. M. Brown, Mesoporous perovskite solar cells and the role of nanoscale compact layers for remarkable all-round high efficiency under both indoor and outdoor illumination, *Nano Energy* 30 (2016) 460–469.
- [29] C.-Y. Chen, J.-H. Chang, K.-M. Chiang, H.-L. Lin, S.-Y. Hsiao, H.-W. Lin, Perovskite photovoltaics for dim-light applications, *Adv. Funct. Mater.* 25 (2015) 7064–7070.
- [30] M. Li, C. Zhao, Z.-K. Wang, C.-C. Zhang, H.K.H. Lee, A. Pockett, J. Barbé, W. C. Tsai, Y.-G. Yang, M.J. Carnie, X.-Y. Gao, W.-X. Yang, J.R. Durrant, L.-S. Liao, S. M. Jain, Interface modification by ionic liquid: a promising candidate for indoor light harvesting and stability improvement of planar perovskite solar cells, *Adv. Energy Mater.* 8 (2018), 1801509.
- [31] J. Dagar, S. Castro-Hermosa, G. Lucarelli, F. Cacialli, T.M. Brown, Highly efficient perovskite solar cells for light harvesting under indoor illumination via solution processed SnO₂/MgO composite electron transport layers, *Nano Energy* 49 (2018) 290–299.
- [32] C.-Y. Chen, W.-H. Lee, S.-Y. Hsiao, W.-L. Tsai, L. Yang, H.-L. Lin, H.-J. Chou, H.-W. Lin, Vacuum-deposited perovskite photovoltaics for highly efficient environmental light energy harvesting, *J. Mater. Chem. A* 7 (2019) 3612–3617.
- [33] R. Cheng, C.-C. Chung, H. Zhang, F. Liu, W.-T. Wang, Z. Zhou, S. Wang, A. B. Djurišić, S.-P. Feng, Tailoring triple-anion Perovskite material for indoor light harvesting with restrained Halide segregation and record high efficiency beyond 36%, *Adv. Energy Mater.* 9 (2019), 1901980.
- [34] S. Castro-Hermosa, G. Lucarelli, M. Top, M. Fahland, J. Fahlteich, T.M. Brown, Perovskite photovoltaics on roll-to-roll coated ultra-thin glass as flexible high-efficiency indoor power generators, *Cell Rep. Phys. Sci.* 1 (2020), 100045.
- [35] A. Babayigit, D. Duy Thanh, A. Ethirajan, J. Manca, M. Muller, H.-G. Boyen, B. Conings, Assessing the toxicity of Pb- and Sn-based perovskite solar cells in model organism *Danio rerio*, *Sci. Rep.* 6 (2016) 18721.
- [36] K. Sharma, V. Sharma, S.S. Sharma, Dye-sensitized solar cells: fundamentals and current status, *Nanoscale Res. Lett.* 13 (2018) 381.
- [37] L.-K. Ma, Y. Chen, P.C.Y. Chow, G. Zhang, J. Huang, C. Ma, J. Zhang, H. Yin, A. M. Hong Cheung, K.S. Wong, S.K. So, H. Yan, High-efficiency indoor organic photovoltaics with a band-aligned interlayer, *Joule* 4 (2020) 1486–1500.
- [38] A.S. Teran, J. Wong, W. Lim, G. Kim, Y. Lee, D. Blaauw, J.D. Phillips, AlGaAs photovoltaics for indoor energy harvesting in mm-scale wireless sensor nodes, *IEEE Trans. Electron Devices* 62 (2015) 2170–2175.
- [39] Y. Cui, Y. Wang, J. Bergqvist, H. Yao, Y. Xu, B. Gao, C. Yang, S. Zhang, O. Inganäs, F. Gao, J. Hou, Wide-gap non-fullerene acceptor enabling high-performance organic photovoltaic cells for indoor applications, *Nat. Energy* 4 (2019) 768–775.
- [40] Y. Zhou, T.M. Khan, J.W. Shim, A. Dindar, C. Fuentes-Hernandez, B. Kippelen, All-plastic solar cells with a high photovoltaic dynamic range, *J. Mater. Chem. A* 2 (2014) 3492–3497.
- [41] W. Shockley, H.J. Queisser, Detailed balance limit of efficiency of p-n junction solar cells, *J. Appl. Phys.* 32 (1961) 510–519.
- [42] Y. Li, N.J. Grabham, S.P. Beeby, M.J. Tudor, The effect of the type of illumination on the energy harvesting performance of solar cells, *Sol. Energy* 111 (2015) 21–29.
- [43] N.H. Reich, W.G.J.H.M. Van Sark, E.A. Alsema, R.W. Lof, R.E.I. Schropp, W. C. Sinke, W.C. Turkenburg, Crystalline silicon cell performance at low light intensities, *Sol. Energy Mater. Sol. Cells* 93 (2009) 1471–1481.
- [44] J. Yuan, Y. Zhang, L. Zhou, G. Zhang, H.-L. Yip, T.-K. Lau, X. Lu, C. Zhu, H. Peng, P.A. Johnson, M. Leclerc, Y. Cao, J. Ulanski, Y. Li, Y. Zou, Single-junction organic solar cell with over 15% efficiency using fused-ring acceptor with electron-deficient core, *Joule* 3 (2019) 1140–1151.
- [45] M. Mainville, M. Leclerc, Recent progress on indoor organic photovoltaics: from molecular design to production scale, *ACS Energy Lett.* 5 (2020) 1186–1197.
- [46] K. Vandewal, K. Tvingstedt, A. Gadisa, O. Inganäs, J.V. Manca, On the origin of the open-circuit voltage of polymer–fullerene solar cells, *Nat. Mater.* 8 (2009) 904–909.
- [47] K. Vandewal, J. Benduhn, V.C. Nikolis, How to determine optical gaps and voltage losses in organic photovoltaic materials, *Sustain. Energy Fuels* 2 (2018) 538–544.
- [48] W. Yang, Y. Luo, P. Guo, H. Sun, Y. Yao, Leakage current induced by energetic disorder in organic bulk heterojunction solar cells: comprehending the ultrahigh loss of open-circuit voltage at low temperatures, *Phys. Rev. Appl.* 7 (2017), 044017.
- [49] Z.-G. Zhang, B. Qi, Z. Jin, D. Chi, Z. Qi, Y. Li, J. Wang, Perylene diimides: a thickness-insensitive cathode interlayer for high performance polymer solar cells, *Energy Environ. Sci.* 7 (2014) 1966–1973.
- [50] N. Li, B.E. Lassiter, R.R. Lunt, G. Wei, S.R. Forrest, Open circuit voltage enhancement due to reduced dark current in small molecule photovoltaic cells, *Appl. Phys. Lett.* 94 (2009), 023307.
- [51] C.M. Proctor, T.-Q. Nguyen, Effect of leakage current and shunt resistance on the light intensity dependence of organic solar cells, *Appl. Phys. Lett.* 106 (2015), 083301.
- [52] R. Steim, T. Ameri, P. Schilinsky, C. Waldauf, G. Dennler, M. Scharber, C. J. Brabec, Organic photovoltaics for low light applications, *Sol. Energy Mater. Sol. Cells* 95 (2011) 3256–3261.
- [53] X. Xu, T. Yu, Z. Bi, W. Ma, Y. Li, Q. Peng, Realizing over 13% efficiency in green-solvent-processed nonfullerene organic solar cells enabled by 1,3,4-thiadiazole-based wide-bandgap copolymers, *Adv. Mater.* 30 (2018), 1703973.
- [54] D. Baran, T. Kirchartz, S. Wheeler, S. Dimitrov, M. Abdelsamie, J. Gorman, R. S. Ashraf, S. Holliday, A. Wadsworth, N. Gasparini, P. Kaienburg, H. Yan, A. Amassian, C.J. Brabec, J.R. Durrant, I. McCulloch, Reduced voltage losses yield 10% efficient fullerene free organic solar cells with >1 V open circuit voltages, *Energy Environ. Sci.* 9 (2016) 3783–3793.
- [55] V. Gupta, A.K.K. Kyaw, D.H. Wang, S. Chand, G.C. Bazan, A.J. Heeger, Barium: an efficient cathode layer for bulk-heterojunction solar cells, *Sci. Rep.* 3 (2013) 1965.
- [56] H.K.H. Lee, Z. Li, J.R. Durrant, W.C. Tsoi, Is organic photovoltaics promising for indoor applications? *Appl. Phys. Lett.* 108 (2016), 253301.
- [57] V. Gupta, A.K. Kyaw, D.H. Wang, S. Chand, G.C. Bazan, A.J. Heeger, Barium: an efficient cathode layer for bulk-heterojunction solar cells, *Sci. Rep.* 3 (2013) 1965.
- [58] T. Fukuhara, Y. Tamai, H. Ohkita, Nongeminate charge recombination in organic photovoltaics, *Sustain. Energy Fuels* 4 (2020) 4321–4351.
- [59] N.K. Elumalai, A. Uddin, Open circuit voltage of organic solar cells: an in-depth review, *Energy Environ. Sci.* 9 (2016) 391–410.
- [60] H.-I. Je, E.-Y. Shin, K.J. Lee, H. Ahn, S. Park, S.H. Im, Y.-H. Kim, H.J. Son, S.-K. Kwon, Understanding the performance of organic photovoltaics under indoor and outdoor conditions: effects of chlorination of donor polymers, *ACS Appl. Mater. Interfaces* 12 (2020) 23181–23189.
- [61] B. Minnaert, P. Veelaert, A proposal for typical artificial light sources for the characterization of indoor photovoltaic applications, *Energies* 7 (2014) 1500–1516.
- [62] W.C. Janglin Chen, Mark Fihn, Handbook of Visual Display Technology, Springer, Berlin, Heidelberg, 2012.
- [63] A.K.K. Kyaw, D.H. Wang, V. Gupta, W.L. Leong, L. Ke, G.C. Bazan, A.J. Heeger, Intensity dependence of current–voltage characteristics and recombination in high-efficiency solution-processed small-molecule solar cells, *ACS Nano* 7 (2013) 4569–4577.
- [64] H.K.H. Lee, J. Wu, J. Barbé, S.M. Jain, S. Wood, E.M. Speller, Z. Li, F.A. Castro, J. R. Durrant, W.C. Tsoi, Organic photovoltaic cells – promising indoor light harvesters for self-sustainable electronics, *J. Mater. Chem. A* 6 (2018) 5618–5626.
- [65] H. Yin, S. Chen, S.H. Cheung, H.W. Li, Y. Xie, S.W. Tsang, X. Zhu, S.K. So, Porphyrin-based thick-film bulk-heterojunction solar cells for indoor light harvesting, *J. Mater. Chem. C* 6 (2018) 9111–9118.
- [66] Y.-J. Heo, Y.-S. Jung, K. Hwang, J.-E. Kim, J.-S. Yeo, S. Lee, Y.-J. Jeon, D. Lee, D.-Y. Kim, Small-molecule organic photovoltaic modules fabricated via halogen-free solvent system with roll-to-roll compatible scalable printing method, *ACS Appl. Mater. Interfaces* 9 (2017) 39519–39525.
- [67] R. Singh, C.L. Chochos, V.G. Gregoriou, A.D. Nega, M. Kim, M. Kumar, S.-C. Shin, S.H. Kim, J.W. Shim, J.-J. Lee, Highly efficient indoor organic solar cells by voltage loss minimization through fine-tuning of polymer structures, *ACS Appl. Mater. Interfaces* 11 (2019) 36905–36916.
- [68] S.-C. Shin, C.W. Koh, P. Vincent, J.S. Goo, J.-H. Bae, J.-J. Lee, C. Shin, H. Kim, H. Y. Woo, J.W. Shim, Ultra-thick semi-crystalline photoactive donor polymer for efficient indoor organic photovoltaics, *Nano Energy* 58 (2019) 466–475.
- [69] J. Wei, C. Zhang, G. Ji, Y. Han, I. Ismail, H. Li, Q. Luo, J. Yang, C.-Q. Ma, Roll-to-roll printed stable and thickness-independent ZnO:PEI composite electron transport layer for inverted organic solar cells, *Sol. Energy* 193 (2019) 102–110.

- [70] N. Gasparini, M. Salvador, T. Heumueller, M. Richter, A. Classen, S. Shrestha, G. J. Matt, S. Holliday, S. Strohm, H.-J. Egelhaaf, A. Wadsworth, D. Baran, I. McCulloch, C.J. Brabec, Polymer: nonfullerene bulk heterojunction solar cells with exceptionally low recombination rates, *Adv. Energy Mater.* 7 (2017), 1701561.
- [71] K. Zhang, Z. Chen, A. Armin, S. Dong, R. Xia, H.-L. Yip, S. Shoaei, F. Huang, Y. Cao, Efficient large area organic solar cells processed by blade-coating with single-component green solvent, *Sol. RRL* 2 (2018), 1700169.
- [72] C.E. Small, S.-W. Tsang, S. Chen, S. Baek, C.M. Amb, J. Subbiah, J.R. Reynolds, F. So, Loss mechanisms in thick-film low-bandgap polymer solar cells, *Adv. Energy Mater.* 3 (2013) 909–916.
- [73] M. Lenes, L.J.A. Koster, V.D. Mihailescu, P.W.M. Blom, Thickness dependence of the efficiency of polymer:fullerene bulk heterojunction solar cells, *Appl. Phys. Lett.* 88 (2006), 243502.
- [74] H.S. Ryu, S.Y. Park, T.H. Lee, J.Y. Kim, H.Y. Woo, Recent progress in indoor organic photovoltaics, *Nanoscale* 12 (2020) 5792–5804.
- [75] R. Arai, S. Furukawa, Y. Hidaka, H. Komiyama, T. Yasuda, High-performance organic energy-harvesting devices and modules for self-sustainable power generation under ambient indoor lighting environments, *ACS Appl. Mater. Interfaces* 11 (2019) 9259–9264.
- [76] S.V. Dayneko, M. Pahlevani, G.C. Welch, Indoor photovoltaics: photoactive material selection, greener ink formulations, and slot-die coated active layers, *ACS Appl. Mater. Interfaces* 11 (2019) 46017–46025.
- [77] M. Ylikunnari, M. Välimäki, K.-L. Väistönen, T.M. Kraft, R. Sliz, G. Corso, R. Po, R. Barbieri, C. Carbonera, G. Gorni, M. Vilkmann, Flexible OPV modules for highly efficient indoor applications, *Flex. Print. Electron.* 5 (2020), 014008.
- [78] S. Mori, T. Gotanda, Y. Nakano, M. Saito, K. Todori, M. Hosoya, Investigation of the organic solar cell characteristics for indoor LED light applications, *Jpn. J. Appl. Phys.* 54 (2015), 071602.
- [79] R. Singh, S.-C. Shin, H. Lee, M. Kim, J.W. Shim, K. Cho, J.-J. Lee, Ternary blend strategy for achieving high-efficiency organic photovoltaic devices for indoor applications, *Chem. – A Eur. J.* 25 (2019) 6154–6161.
- [80] Y. Cui, H. Yao, T. Zhang, L. Hong, B. Gao, K. Xian, J. Qin, J. Hou, 1 cm² organic photovoltaic cells for indoor application with over 20% efficiency, *Adv. Mater.* 31 (2019), 1904512.
- [81] Y. Lin, J. Wang, Z.-G. Zhang, H. Bai, Y. Li, D. Zhu, X. Zhan, An electron acceptor challenging fullerenes for efficient polymer solar cells, *Adv. Mater.* 27 (2015) 1170–1174.
- [82] A. Wadsworth, M. Moser, A. Marks, M.S. Little, N. Gasparini, C.J. Brabec, D. Baran, I. McCulloch, Critical review of the molecular design progress in nonfullerene electron acceptors towards commercially viable organic solar cells, *Chem. Soc. Rev.* 48 (2019) 1596–1625.
- [83] G. Zhang, J. Zhao, P.C.Y. Chow, K. Jiang, J. Zhang, Z. Zhu, J. Zhang, F. Huang, H. Yan, Nonfullerene acceptor molecules for bulk heterojunction organic solar cells, *Chem. Rev.* 118 (2018) 3447–3507.
- [84] P. Cheng, G. Li, X. Zhan, Y. Yang, Next-generation organic photovoltaics based on nonfullerene acceptors, *Nat. Photonics* 12 (2018) 131–142.
- [85] Y. Lin, Z.-G. Zhang, H. Bai, J. Wang, Y. Yao, Y. Li, D. Zhu, X. Zhan, High-performance fullerene-free polymer solar cells with 6.31% efficiency, *Energy Environ. Sci.* 8 (2015) 610–616.
- [86] Y. Lin, Q. He, F. Zhao, L. Huo, J. Mai, X. Lu, C.-J. Su, T. Li, J. Wang, J. Zhu, Y. Sun, C. Wang, X. Zhan, A facile planar fused-ring electron acceptor for as-cast polymer solar cells with 8.71% efficiency, *J. Am. Chem. Soc.* 138 (2016) 2973–2976.
- [87] Z. Ding, R. Zhao, Y. Yu, J. Liu, All-polymer indoor photovoltaics with high open-circuit voltage, *J. Mater. Chem. A* 7 (2019) 26533–26539.
- [88] C.-Y. Liao, Y. Chen, C.-C. Lee, G. Wang, N.-W. Teng, C.-H. Lee, W.-L. Li, Y.-K. Chen, C.-H. Li, H.-L. Ho, P.H.-S. Tan, B. Wang, Y.-C. Huang, R.M. Young, M. R. Wasielewski, T.J. Marks, Y.-M. Chang, A. Facchetti, Processing strategies for an organic photovoltaic module with over 10% efficiency, *Joule* 4 (2020) 189–206.
- [89] P. Bi, X. Hao, Versatile ternary approach for novel organic solar cells: a review, *Sol. RRL* 3 (2019), 1800263.
- [90] L. Lu, T. Xu, W. Chen, E.S. Landry, L. Yu, Ternary blend polymer solar cells with enhanced power conversion efficiency, *Nat. Photonics* 8 (2014) 716–722.
- [91] M. Nam, M. Cha, H.H. Lee, K. Hur, K.-T. Lee, J. Yoo, I.K. Han, S.J. Kwon, D.-H. Ko, Long-term efficient organic photovoltaics based on quaternary bulk heterojunctions, *Nat. Commun.* 8 (2017) 14068.
- [92] M. Nam, H.Y. Noh, J. Cho, Y. Park, S.-C. Shin, J.-A. Kim, J. Kim, H.H. Lee, J. W. Shim, D.-H. Ko, All-day operating quaternary blend organic photovoltaics, *Adv. Funct. Mater.* 29 (2019), 1900154.
- [93] R. Yu, H. Yao, J. Hou, Recent progress in ternary organic solar cells based on nonfullerene acceptors, *Adv. Energy Mater.* 8 (2018), 1702814.
- [94] C.H.Y. Ho, S.H. Cheung, H.-W. Li, K.L. Chiu, Y. Cheng, H. Yin, M.H. Chan, F. So, S.-W. Tsang, S.K. So, Using ultralow dosages of electron acceptor to reveal the early stage donor–acceptor electronic interactions in bulk heterojunction blends, *Adv. Energy Mater.* 7 (2017), 1602360.
- [95] J.-M. Costantini, G. Lelong, M. Guillaumet, W.J. Weber, S. Takaki, K. Yasuda, Color-center production and recovery in electron-irradiated magnesium aluminate spinel and ceria, *J. Phys.: Condens. Matter* 28 (2016), 325901.
- [96] M. Nam, J.-H. Kang, J. Shin, J. Na, Y. Park, J. Cho, B. Kim, H.H. Lee, R. Chang, D.-H. Ko, Ternary organic blend approaches for high photovoltaic performance in versatile applications, *Adv. Energy Mater.* 9 (2019), 1901856.
- [97] C. Wang, X. Xu, W. Zhang, S.B. Dkhil, X. Meng, X. Liu, O. Margeat, A. Yartsev, W. Ma, J. Ackermann, E. Wang, M. Fahlman, Ternary organic solar cells with enhanced open circuit voltage, *Nano Energy* 37 (2017) 24–31.
- [98] Y. Cho, T. Kumari, S. Jeong, S.M. Lee, M. Jeong, B. Lee, J. Oh, Y. Zhang, B. Huang, L. Chen, C. Yang, Guest-oriented nonfullerene acceptors for ternary organic solar cells with over 16.0% and 22.7% efficiencies under one-sun and indoor light, *Nano Energy* 75 (2020), 104896.
- [99] S. Li, L. Ye, W. Zhao, S. Zhang, S. Mukherjee, H. Ade, J. Hou, Energy-level modulation of small-molecule electron acceptors to achieve over 12% efficiency in polymer solar cells, *Adv. Mater.* 28 (2016) 9423–9429.
- [100] S. Li, L. Ye, W. Zhao, S. Zhang, H. Ade, J. Hou, Significant influence of the methoxyl substitution position on optoelectronic properties and molecular packing of small-molecule electron acceptors for photovoltaic cells, *Adv. Energy Mater.* 7 (2017), 1700183.
- [101] K. Yang, Q. Liao, C.W. Koh, J. Chen, M. Su, X. Zhou, Y. Tang, Y. Wang, Y. Zhang, H.Y. Woo, X. Guo, Improved photovoltaic performance of a nonfullerene acceptor based on a benzo[b]thiophene fused end group with extended π-conjugation, *J. Mater. Chem. A* 7 (2019) 9822–9830.
- [102] W. Wang, B. Zhao, Z. Cong, Y. Xie, H. Wu, Q. Liang, S. Liu, F. Liu, C. Gao, H. Wu, Y. Cao, Nonfullerene polymer solar cells based on a main-chain twisted low-bandgap acceptor with power conversion efficiency of 13.2%, *ACS Energy Lett.* 3 (2018) 1499–1507.
- [103] J. Roncali, Molecular engineering of the band gap of π-conjugated systems: facing technological applications, *Macromol. Rapid Commun.* 28 (2007) 1761–1775.
- [104] M.A. Alamoudi, J.I. Khan, Y. Firdaus, K. Wang, D. Andrienko, P.M. Beaujuge, F. Laquai, Impact of nonfullerene acceptor core structure on the photophysics and efficiency of polymer solar cells, *ACS Energy Lett.* 3 (2018) 802–811.
- [105] Record: 26% efficiency in a low-light environment for the solar technology of ARMOR solar power films. 2020; Available from: <<https://en.asca.com/latest-news/record-26-efficiency-in-a-low-light-environment-for-the-solar-technology-of-armor-solar-power-films/>>.

Lin Xie began in 2019 her Doctoral Training Partnership (DTP) PhD studies in chemical engineering at Ningbo Institute of Materials Technology, Chinese Academy of Science and Engineering and University of Nottingham Ningbo China (UNNC) under the supervision of Professor Ziyi Ge, Tao Wu and Bencan Tang. She received her MS from University College London and bachelor from UNNC. Her research focuses on high-efficient organic photovoltaics.



Wei Song received his bachelor's degree from Hefei University of Technology in 2016. He further got his master's degree in Shanghai University in 2019. He is currently pursuing his Ph.D. under the supervision of Prof. Ziyi Ge in Ningbo Institute of Materials Technology and Engineering, Chinese Academy of Science. His research interests mainly focus on the development of flexible conducting materials for wearable organic photovoltaic.



Jinfeng Ge received his master's degree in Beijing University of Chemical Technology in 2020, and now he is a Ph.D. student under the supervision of Prof. Ziyi Ge at Ningbo Institute of Materials Technology and Engineering, Chinese Academy of Science. His research interests mainly focus on nonfullerene all-small-molecule organic solar cells.





Dr Bencan Tang received her Ph.D. from the University of Nottingham. She conducted her postdoctoral research in the University of Southampton, UK (2009–2011). Currently, she is the associate professor in the University of Nottingham Ningbo China. Her expertise lies in the construction of complex molecules, both computationally and experimentally.



Professor Tao Wu, a Fellow of the British Royal Society of Chemistry, is also Dean of the Faculty of Science and Engineering in the University of Nottingham Ningbo China, and Dean of Ningbo Nottingham New Material Research Technology Institute. He has over 25 years of experience on the efficient conversion and utilization of fossil fuels and biomass. His research programs cover a wide range from blue-sky research to proof of concept and patent development leading to commercialization. He has completed over 40 research projects funded by both agencies and industry.



Dr Xiaoli Zhang with a B.Sc. in Chemistry from Shandong University (China), obtained her M.Sc. and PhD in Material Chemistry under Professor Young Soo Kang at Pukyong National University (South Korea). Upon completion of her PhD, she worked as a research fellow at Monash University (Australia) with Professor Udo Bach and Professor Yi-Bing Cheng on Photovoltaic Materials and Devices (2008–2011). She worked with Professor Zheng Xiao Guo at the University College London (UK) on material synthesis and simulation of energy conversion (2014–2015), before taking a full faculty position at Zhengzhou University (China) in 2016.



Professor Ziyi Ge received his Ph.D. from Institute of Chemistry, Chinese Academy of Sciences in 2004. He conducted his postdoctoral research on organic electronics in Tokyo Institute of Technology, Kanagawa University, Japan and the University of New South Wales, Australia during 2005–2009. Currently, he is the leader of Organic Electronic Material and Device Group at Ningbo Institute of Material Technology and Engineering, Chinese Academy of Sciences. His research interests focus on organic/perovskite solar cells and OLEDs.